JAERI-M
84-133

PROGRESS REPORT ON SAFETY RESEARCH OF HIGH-LEVEL WASTE MANAGEMENT FOR THE PERIOD APRIL 1983 TO MARCH 1984

June 1984

(Eds.) Haruto NAKAMURA and Shingo TASHIRO

日本原子力研究所
Japan Atomic Energy Research Institute

JAERI-M レポートは，日本原子力研究所が不定期に公刊している研究報告書です。
入手の問合わせは，日本原子力研究所技術情報部情報資料課（〒319—11 茨城県那珂郡東海村）あて，お申しこしください。なお，このほかに財団法人原子力弘済会資料センター（〒319—11 茨城県那珂郡東海村日本原子力研究所内）で複写による実費頒布をおこなっております。

JAERI-M reports are issued irregularly.
Inquiries about availability of the reports should be addressed to Information Section, Division of Technical Information, Japan Atomic Energy Research Institute, Tokai-mura, Naka-gun, Ibaraki-ken 319—11, Japan.

編集兼発行　日本原子力研究所
印　　刷　日立高速印刷株式会社

JAERI-M 84-133

Progress Report on Safety Research of High-Level Waste Management for the Period April 1983 to March 1984.

Haruto NAKAMURA and Shingo TASHIRO

Department of Environmental Safety Research
Tokai Research Establishment, JAERI

(Received June 28, 1984)

Safety research on high level waste management in the fiscal year of 1983 is reviewed.

Topics are as follows;

1) Waste Safety Testing Facility (WASTEF) has been full operated. Durability tests of vitrified waste form were started and the characteristics of the forms necessary for safety assessment of storage facility were evaluated by using radioactive materials.

2) Information regarding characteristics of deep underground rock mass has been collected in underground facilities.

3) Glass waste forms were examined with emphasis on leaching mechanisms to predict the long term durability.

Keywords: High-level Waste, WASTEF, Progress, Durability, Leaching Mechanism, Safety Assessment,

JAERI-M 84-133

1983年4月より1984年3月までの高レベル廃棄物処理処分の安全性研究に関するプログレスレポート

日本原子力研究所東海研究所環境安全研究部
中村　治人・田代　晋吾

（１９８４年６月２８日受理）

1983年度の高レベル廃棄物処理処分の安全性研究の進捗状況をまとめたものである。主な点は次の通りである。

1）　廃棄物安全試験施設（ＷＡＳＴＥＦ）が完全稼動に入った。ガラス固化体の耐久性試験が開始され，貯蔵施設の安全性評価に必要な固化体の性質の評価が放射性物質を使って行われた。

2）　深地層における岩盤の性質に関する情報を地下施設から集めた。

3）　長期耐久性を予測するため，浸出機構に重点を置いてガラス固化体の性能試験を行った。

Contents

Introduction

The Japan Atomic Energy Research Institute (JAERI) plays a role in the safety studies and development of new technologies on the national program of high level waste management. This report reviews main results obtained in the fiscal year of 1983 following the progress report of 1981 (JAERI-M 82-145) and 1982 (JAERI-M 83-076).

Topics are as follows;

1. The waste Safety Testing Facility (WASTEF) has been full operated and safety examinations of glass waste forms have been carried out by using radioactive samples.
2. In order to obtain general information regarding characteristics of deep underground rock mass, permeability data and core samples were collected from underground facilities at various sites. The underground experiments in a metal mine was continued and a new facility was constructed in a granite rock mass in near surface.
3. Glass waste forms were examined with emphasis on leaching mechanisms to predict the long term durability. Materials in grain boundary of SYNROCK were studied as critical materials to control the leach rate.

1. Waste Forms Examination

T. Banba

One of the most important functions of the waste forms is to provide the initial barrier against radionuclide release in a repository. Glass waste form was examined with emphasis on the leaching mechanisms to predict the long-term leach rates. The distribution of elements in the surface layers formed during leaching was examined and leahing mechanisms of each element were discussed.

Under the conditions of a underground repository, the extent of leaching of glass waste form may be small, which means that it is necessary to develop special techniques in order to estimate the leach rates of glass waste form. Our experiments suggested that the surface analysis by SEM-EDX was useful for the estimation of the leach rates when the extent of leaching was small.

Crystalline phases in a devitrified glass containing platinum group elements were studied. Seven crystalline phases, i.e., (RE)$BSiO_5$, (RE,Sr,Ba)MoO_4, (RE)PO_4, CeO_2, SiO_2, (Ru,Rh)O_2 and (Pd,Rh,Te), were identified by X-ray and electron diffraction methods.

SYNROC waste form is one of the most feasible alternatives because of low leachability. Microstructure of SYNROC synthesized by three different method was studied. All samples contained amorphous phase whose content depended on each synthesis method.

1.1 The characteristics of surface layers of a glass waste form

T. Murakami and T. Banba

Introduction

The most possible release of radionuclides from glass waste forms is by leaching through water. Therefore an important subject for the safety evaluation of the glass waste forms is prediction of the leaching behavior, especially, the long-term leaching behavior of the glass waste forms from short-term laboratory experiments. This is the reason why the leaching mechanisms, which are considered to give a key for the prediction, have been studied intensively (see, for example, Refs. 1 and 2). The leaching mechanisms are complicated because leaching is affected by such factors as glass compositions, surface area to solution volume, solution pH, temperature, solubility limit and so on[3]. They are further complicated by formation of the surface layers which usually form on the glass waste forms during leaching. Hench et al. have already pointed out that the formation of the surface layers has an influence on the leaching mechanisms[1]. It should be then examined how the formation affects the leaching mechanisms. At the first stage of the above examination, the characteristics of the surface layers on the glass waste forms including crystallization should be understood. The Soxhlet type leach test was chosen to obtain thick surface layers in short time for examination of the characteristics of the surface layers.

Experimental

The glass waste form used for this study was a borosilicate glass (J-10)[4] and contained 14 wt% nonradioactive simulated waste oxides[5]. The glass waste form was prepared as follows: 1. Nonradioactive waste oxides, which were preliminarily calcined at 650°C for 2 hours, were mixed with a glass frit. 2. The mixture was melted at 1150° for 1.5 hour. 3. The molten glass was quenched and kept at 500°C for one hour and then it was cooled to room temperature slowly. Table I gives the composition of the glass waste form.

The glass waste form was cut into a block specimen of $7.3 \times 6.5 \times 4.5$ mm in size and 0.5694 gram in weight. Soxhlet leach test was carried out at 100°C for 200 days using the block specimen.

After observed by optical microscopy, the leached glass was mounted in resin, sectioned and polished. Characteristics of the surface layers were examined by optical microscopy, SEM (scanning electron microscopy), SEM-EDX (energy dispersive X-ray spectroscopy) and SEM-WDX (wavelength dispersive X-ray spectroscopy). Portion of the surface layers was ground to powder for observation of fine texture of the surface layers, identification of crystalline phases in the surface layers and elemental analysis of the crystalline phases, which were made by AEM (analytical electron microscopy).

Results

Morphological and textural observation of the surface layers

The thickness of the surface layers was around 0.5 mm and the leached part of the block specimen was reduced to 2/3 of the same part of the block specimen before the leach test. The surface layers were so fragile that they were broken easily by picking with a needle.

An optical micrograph and an SEM micrograph of the polished surface of the surface layers are shown in Fig. 1(A) and (b), respectively. The surface layers are divided into four parts morphologically; an innermost layer, A, 70 μm in thickness; an inner layer, B, 90 μm; an outer layer, C, 140 μm; an outermost layer, D, 220 μm. The thickness of each layer varied from one part to another slightly. The results of the classification of the surface layers are summarized in Fig. 1(C) schematically. A transmission electron micrograph (Photo. 2a of Ref. 6) reveals that the surface layers are composed by very small crystalline and noncrystalline particles of around 100 to 1000 Å.

Elemental analysis of the surface layers

Compositional analysis of the surface layers was carried out by means of SEM-EDX and the results are given in Table II. This analysis could not yield accurate quantitative analysis because of different roughness of the surface layers but the results are useful enough for the following discussion.

The elements in the surface layers are classified into three groups according to their compositional changes in the four layers and the glass.

Group I: alkali metals such as Na, K and Cs. Almost all are leached out from the surface layers, so they are not found there. Group II: Mn, Fe, Ni, Zr, La and Ce. Larger amounts are contained in the surface layers than in the unleached part of the specimen. Their concentrations are the highest in the D layer and decrease in the order of D > C > B > A. However, compositional difference between the A and B layers is small. Group III: those which do not belong to the group I nor II. They are alkaline earths such as Mg, Ca and Ba and network formers such as Si and Al. The alkaline earths do not have a similar tendency with each other in terms of compositional changes in the layers and the glass. In general, larger amounts of Mg and Ba are found in the surface layers than in the unleached part of the specimen and smaller amounts of Ca, in the surface layers like those of Al and Si.

Qualitative analysis by SEM-WDX was carried out for the elements which could not be analyzed by SEM-EDX because of the inability of resolution and detection. The results revealed that Cr, Te, Co, Gd, Y, Sm, Pr and Dy occurred in the surface layers and their distribution among the layers showed a similar tendency as that of group II. Trace amounts of Ti, Ag, Cd and Cs were found but Mo, Rb and Sr were not detected. The result of Mo by WDX was inconsistent with that by EDX.

A crystalline phase in the surface layers

The AEM analyses revealed that the crystalline phase in the surface layers occurred as a sheet silicate alone which was rich in Si and Fe and also contains Mg, Al, Zr, Mn, Ca, Ba, La, Ce, Nd, Ni and Cl. Some specimens included K, Sm, Co or Mo besides the above elements. The concentrations of the above elements varied from one specimen to another slightly. The detailed procedure of the analyses has been already reported elsewhere[6,7].

Discussion

Multilayered structure developed in the surface layers

The fine particles of 100 to 1000 Å are considered to form as a result of recrystallization and decomposition of the glass during leaching. The fine particles are mixture of crystalline and noncrystalline materials and

constitute a layer. The surface layers consist of four layers and thus have multilayered structure.

Allen[8] and Malow[9] described the multilayered structure of surface layers. Allen observed the natural basaltic glass and pointed out that the cycles of wetting and dehydration in nature made the multilayered structure. In Malow's case, his experiments were carried out in a closed autoclave and so the multilayered structure might be caused by change of the leaching conditions, for example, change of the nature of leachant during leach test. In contrast with their cases, leach test of the Soxhlet type was carried out in this study. Accordingly, there must not occur periodic nor discontinuous change of the leachant during leach test. The surface layers have, however, the discontinuous multilayered structure compositionally and morphologically in spite of the continuous leaching condition.

Since the formation of crystalline phases regulates solution concentrations[10], the formation of the discontinuous surface layers under the continuous leaching condition may result from local change of the nature of solution. However, we have not had any evidence for such local change at the present stage.

Behavior of elements in the surface layers

The shrinkage of the surface layers occurred easily because of drying during sample preparation mainly and reconstruction of the layers during leaching secondarily. Namely, the shrinkage made the apparent concentrations of the elements high in the surface layers. In order to compare the cencentrations of the elements in the layers and the glass each other effectively, the compositions of the surface layers in Table II were normalized. The concentrations of Fe_2O_3 were used for normalized factors due to the following reasons: 1. Almost all iron ions remained in the surface layers because they were not found in the leachates [14]. 2. The errors by normalization would be minimized because the concentration of Fe_2O_3 was rather high in the as-prepared glass (Table II). The assumption for normalization was that Fe was immobile and Fe did not move from layer to layer during leaching, i.e., the concentration of Fe_2O_3 was 4.13 wt% in any layer. The normalization was carried out according to the following equation,

$$ {}_{L}C_{E} = {}_{L}A_{E} \frac{C_{Fe}}{{}_{L}A_{Fe}} \quad (wt\%) , $$

where ${}_{L}C_{E}$ is the normalized concentration of the oxide, E, in the layer, L, ${}_{L}A_{E}$ is the apparent concentration of the oxide, E, in the layer, L, which is given in Table II, ${}_{G}C_{Fe}$ is the concentration of Fe_2O_3 in the as-prepared glass, which is 4.13 wt%, and ${}_{L}A_{Fe}$ is the apparent concentration of Fe_2O_3 in the layer, L (Table II). The results are listed in Table III which makes the behavior of elements in the surface layers clear.

The elements of group I show the same feature as discussed before. Since most of Mo is depleted from the layers, Mo may belong to this group. The behavior of the elements of group II and III, however, looks different from that without normalization.

The concentrations of the elements of group II are almost constant throughout the layers and they are nearly equal to those in the as-prepared glass within experimental errors except those of Mn and Ce. This means that these elements are immobile and there occurs little diffusion of those elements in the layers and glass. This result makes us confirm that the apparent high concentrations of the elements of group II are caused by shrinkage of the layers. Although there remains a little ambiguity with respect to the behavior of Ce and Mn, their high concentrations in the layers and the fact that they are constituents of the sheet silicate support that Ce and Mn belong to group II.

The elements of group III are further divided into two subgroups; one is group IIIa to which Si, Al and Ca belong and the other is group IIIb to which Mg and Ba belong. The concentrations of the elements of group IIIa are significantly lower in the layers than in the as-prepared glass. They decrease in the order of A $\simeq$ B > C > D generally, in the surface layers. This means that the elements of group IIIa are mobile and diffuse through the glass and the layers.

The concentration gradients of Mg and Ba across the layers are different from those of the elements of group II (Table III). The concentrations of Mg are higher in the two middle layers than in the A and D layers, and those of Ba are higher in the inner layer than in the outer layer. This means that the elements of group IIIb diffuse a little and they are almost immobile. The behavior of Ba in the layers is pressumed to be complicated considering leachability of Ba[11].

Effects of the formation of the sheet silicate on leaching

We cannot identify, at the present stage, which sheet silicate the crystalline phase in the surface layers belongs to, but the results of the elemental analysis give sufficient information for crystal-chemical examination. The sheet silicate which contains such a wide range of cations has a chemical form of $A_xB_y(Si, Al)_z(O, OH)_m$ where x, y and z are given figures and m is a given integer and the sheet silicate may also contain $n \cdot H_2O$[12]. The sites for A cations are located at the interstices between the two-dimensional network of the linked tetrahedra and accommodate large cations more than 1 Å in ion radius such as Ca, Ba and rare earths. The sites for B cations are octahedral ones which are occupied by intermediate cations such as Mn, Fe, Zr, Mg, Ni and Al. The linked tetrahedra are formed by small cations such as Si and Al. The above chemical form is accordingly rewritten as follows; $(Ca, Ba, La, Ce, Nd)_x$ $(Mn, Fe, Zr, Mg, Ni, Al)_y(Si, Al)_z(O, OH)_m$. The variation of the cell dimensions mentioned above is due to the difference of the values of x, y and z of the crystal particles.

Since the sheet silicate can accommodate large to small cations, the leaching mechanisms must be different from those without the formation of the sheet silicate. Leachability of a given element must be lower, in general, when the element enters the sheet silicate. For example, Ba remains in the layers because of the formation of the sheet silicate in this study while Ba is poor in the layers or depleted from the layers in the other studies[9,13]. The elements of group II and III might likewise give different leachability without the formation of the sheet silicate.

Potasium was found in only one sheet silicate particle and Na and Cs were not found in any particle. Monovalent cations such as K and Na are accommodated in the A sites in natural sheet silicates[12]. However, it is considered that monovalent cations in this study do not enter the sheet silicate maybe due to the pH conditions and so on in the layers. The formation of the sheet silicate does not have any influence on the leaching behavior of monovalent cations.

The sheet silicate alone forms in this study but it is possible that other crystalline phases form under different experimental conditions. This means that they are the elements of group II and III that are accommodated in the sheet silicate and remain in the surface layers in this

study but different elements may remain in surface layers corresponding to the formation of different kinds of crystalline phases.

References

1. L.L. Hench, D. E. Clark and E. L. Yen-Bower, "Corrosion of Glasses and Glass-Ceramics, "Nucl. Chem. Waste Manage., 1, 59 (1980).
2. B. T. Kenna, "Analysis of Long-Term Soxleht Tests," Nucl. Chem. Waste Manage., 3, 69 (1982).
3. D. E. Clark and L. L. Hench, "An Overview of the Physical Characterization of Leached Surfaces, "Nucl. Chem. Waste Manage., 2, 93 (1981).
4. T. Banba and S. Tashiro, "Safety Evaluation of Simulated High-Level Waste Glass Products (I) (Thermal Stability)," JAERI-M 8706, Japan Atomic Energy Research Institute, Tokai, Ibaraki (1980).
5. T. Banba, H. Kimura, H. Kamizono and S. Tashiro, "Simulated HLW Compositions for Cold Test of Waste Management Development," JAERI-M 82-088, Japan Atomic Energy Research Institute, Tokai, Ibaraki (1982).
6. T. Murakami and T. Banba, "Crystalline phase in surface Layers of Glass Waste Form," J. Nucl. Sci. Technol., 20, 614 (1983).
7. H. Nakamura and S. Tashiro, "Progress Report on Safety Research of High-Level Waste Management for the period April, 1982 to March, 1983", JAERI-M 83-076 (1983).
8. C. C. Allen, "Stability and Alteration of Naturally Occurring Low-Silica Glasses: Implications for the Long-Term Stability of Waste Form Glasses," Scientific Basis for Nuclear Waste Management V, p.37, W. Lutze, Ed., North-Holland, New York (1982).
9. G. Malow, "The Mechanisms for Hydrothermal Leaching of Nulcear Waste Glasses: Properties and Evaluation of Surface Layers," Scientific Basis for Nuclear Waste Management V, p.25, W. Lutze, Ed., North-Holland, New York (1982).
10. B. Grambow, "The Role of Metal Ion Solubility in Leaching of Nuclear Waste Glasses," Scientific Basis for Nuclear Waste Management V, p.93, W. Lutze, Ed., North-Holland, New York (1982).
11. T. Banba and T. Murakami, "The Leading Mechanisms of a Glass Waste form," in this report.

12. L. Bragg and G. F. Claringbull, Crystal Structures of Minerals, G. Bell and Sons Ltd., London (1965).

13. F. K. Altenhein, W. Lutze and G. Malow, "The Mechanisms for Hydrothermal Leaching of Glass and Glass-Ceramic Nuclear Waste Forms," Scientific Basis for Nuclear Waste Management III, p.363, J. G. Moore, Ed., Plenum Press, New, York (1981).

TABLE I Composition of glass waste form

Component	Content(wt%)	Component	Content(wt%)
Additive		Waste	
SiO_2	(38.3)[b]	Cr_2O_3	0.20
B_2O_3	11.8	CoO	0.09
Al_2O_3	7.38	NiO	0.42
Na_2O[a]	20.3	Ag_2O	(0.02)
K_2O	(1.14)	CdO	(0.02)
MgO	0.84	TeO_2	(0.17)
CaO	6.43	Cs_2O	0.72
TiO_2	0.09	Ce_2O_3	(1.13)
P_2O_5[a]	0.25	Nd_2O_3	(0.73)
		La_2O_3	(0.35)
Waste		Sm_2O_3	0.30
SrO	0.24	Y_2O_3	0.25
BaO	0.48	Pr_2O_3	(0.17)
Fe_2O_3[a]	4.13	Dy_2O_3	0.16
MnO_2[a]	0.22	Tb_2O_3	(0.04)
ZrO_2	1.05	Er_2O_3	(0.03)
Rb_2O	(0.10)	Gd_2O_3	(0.31)
MoO_3	1.37		

[a]Component contained in both additive and waste.

[b]Values in parentheses are calculated ones.

TABLE II Comparison of compositions of surface layers with those of unleached part of specimen and as-prepared glass (wt%)[a]

Group	Oxide	As-prepared glass[b]	Unleached part of specimen	Layer			
				A	B	C	D
I	Na_2O	20.03	21.9	ND	ND	ND	ND
	K_2O	(1.14)	1.0	ND	ND	ND	ND
	Cs_2O	0.72	P	ND	ND	ND	ND
	MoO_3	1.37	1.4	0.3	ND	0.2	0.7
II	Fe_2O_3	4.13	3.9	8.7	8.9	12.2	15.9
	NiO	0.42	0.4	0.7	1.1	1.7	2.4
	ZrO_2	1.05	1.1	2.2	2.5	3.3	4.0
	La_2O_3	(0.35)	ND	0.6	0.9	1.1	1.0
	Ce_2O_3	(1.13)	0.7	1.5	1.3	2.0	3.0
	Nd_2O_3	(0.73)	P	P	P	P	P
	MnO	0.22	ND	1.4	1.4	1.9	2.6
III	SiO_2	(38.3)	38.5	32.3	39.9	25.1	14.7
	Al_2O_3	7.38	7.1	4.0	4.7	5.3	3.7
	CaO	6.43	7.0	2.5	2.2	1.6	1.3
	MgO	0.84	1.0	1.3	2.5	3.1	1.9
	BaO	0.48	ND	1.4	1.3	1.3	1.2

[a] Values should be treated as semi-quantitative ones (see text). The ares for analyses are squares of 20 to 30 μm in one edge. Although Nd was found in any layer, analysis of Nd could not be carried out owing to lack of Nd standard. Standard of Cs could not be prepared. ND; none detected, P; present.

[b] Values from TABLE I. Values in parentheses are calculated ones.

TABLE III Normalized compositions of surface layers and compositions of unleached part of specimen and as-prepared glass (wt%)[a]

Group	Oxide	As-prepared glass[b]	Unleached part of specimen[b]	Layer			
				A	B	C	D
I	Na_2O	20.03	21.9	ND	ND	ND	ND
	K_2O	(1.14)	1.0	ND	ND	ND	ND
	Cs_2O	0.72	P	ND	ND	ND	ND
	MoO_3	1.37	1.4	0.1	ND	0.1	0.2
II	Fe_2O_3	4.13	3.9	4.13	4.13	4.13	4.13
	NiO	0.42	0.4	0.3	0.5	0.6	0.6
	ZrO_2	1.05	1.1	1.0	1.2	1.1	1.0
	La_2O_3	(0.35)	ND	0.3	0.4	0.4	0.3
	Ce_2O_3	(1.13)	0.7	0.7	0.6	0.7	0.8
	MnO	0.22	ND	0.7	0.6	0.6	0.7
IIIa	SiO_2	(38.3)	38.5	15.3	18.5	8.5	3.8
	Al_2O_3	7.38	7.1	1.9	2.2	1.8	1.0
	CaO	6.43	7.0	1.2	1.0	0.5	0.3
IIIb	MgO	0.84	1.0	0.6	1.2	1.0	0.5
	BaO	0.48	ND	0.7	0.6	0.4	0.3

[a] See text for normalization method. ND; none detected, P; present.

[b] Values from TABLE II. Values in parentheses are calculated ones.

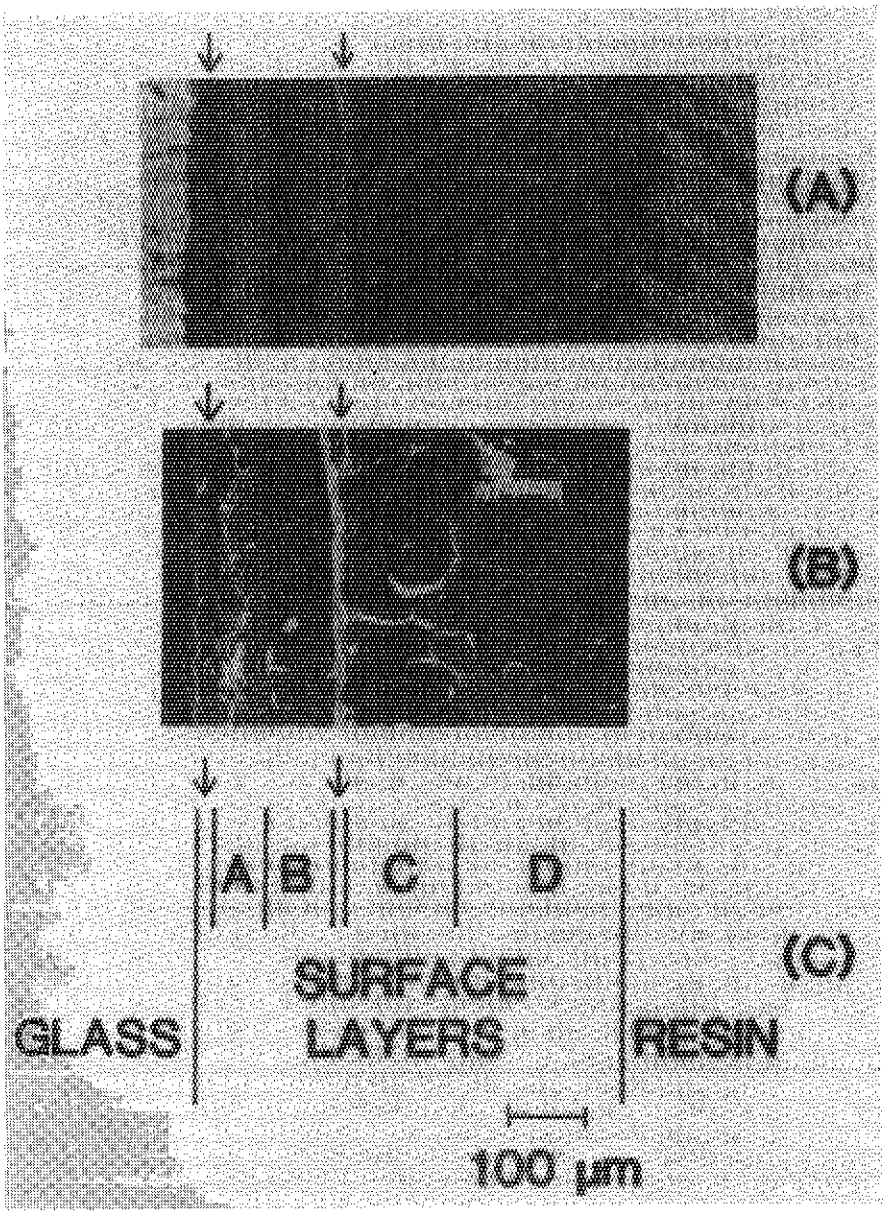

Fig. 1 (A) Optical micrograph and (B) scanning electron micrograph of polished surface of surface layers. (C) Schematical diagram of (A) and (B). The areas in (A), (B) and (C) are correspond to each other. Arrows indicate the two large cracks. Many small cracks are also observed.

1.2 The Leaching Mechanisms of a Glass Waste Form

T. Banba

INTRODUCTION

Since the radionuclides are most likely to be released from the glass waste forms by leaching through water, prediction of leach rates, especially in long-term, is one of the most important subjects to be examined. The long-term leach rates can be derived from the clarification of leaching mechanisms based on the short-term experiments in laboratory.

The leaching mechanisms have been studied by many authors(see, for example, Ref. 1 and 2). The mechanisms are still obscure with respect to the concrete relevance of the surface layers to leaching. To clarify the leaching mechanisms, the Soxhlet type leach test was carried out and we examined alteration of the glass waste form, especially the surface layers[3]. In the present paper, we analyzed the leaching solutions and the leaching mechanisms were elucidated based on the leach rates of the glass waste form and examination of the surface layers.

EXPERIMENTAL

The glass waste form used for this study was a borosilicate glass(J-10)[4] with 14 wt% non-radioactive simulated waste oxides.

The composition of the glass waste form is given in Table I. The glass was cut into a block specimen of 7.3 x 6.5 x 4.5 mm in size and 0.5694 gram in weight.

The leaching experiment was carried out at 100°C for 200 days by using a Soxhlet leach test apparatus made of quartz glass. Leaching solution was replaced by new one and analyzed at the following time intervals; every day for the first week, every other day for the following two weeks, once per a week for the following six weeks, once per two weeks for the following ten weeks. At the end of the experiment, the block specimen was slowly cooled in air. The leaching solutions were quantitatively analyzed by inductively coupled plasma atomic emission spectroscopy(ICP) and flame atomic absorption spectroscopy(FAA).

RESULTS

Unleached part of the block specimen after leaching was 5.7 x 4.9 x 2.9 mm in size and 0.3569 gram in weight. The leach rate of the glass is represented by elemental fractional release, which is expressed by the following equation.

$$FL_i = \sum_j w_{i,j} / W_i \qquad (1)$$

where $w_{i,j}$ is the weight of element i in the leaching solution j

and W_i is the initial weight of element i in the specimen. Table II summarizes results of the fractional release. Ten elements, Cs, B, Mo, Na, Ba, Sr, Ca, Cr, Al and Mg, were quantitatively measured by ICP and FAA, but concentrations of Y and Zr were too small to obtain quantitative data. Concentrations of Mn, Fe, Ni and rare earth elements(La, Ce, Nd, Sm, Dy) in the solutions were under the detection limits by ICP. Using a quartz leach test apparatus, no quantitative analysis of Si could be carried out. Time dependency of the fractional releases of Cs, B, Mo and Na are shown in Fig. 1, and that of Ba, Sr, Ca, Cr, Al and Mg are shown in Fig. 2.

For Cs, B, Mo and Na, the relationship between the fractional releases and time can be approximated by the following equation; $\log(FL_i) = n \log(\text{time}) + A$, where n represents a slope and A is a constant. The n value is about 0.85 for the above elements. Theoretically, n = 0.5 for diffusion controlled mechanisms and n = 1.0 in the event of congruent dissolution[5]. The n value in present study, 0.85, indicates that the leaching of these elements are complex involving both decomposition of the glass matrix and diffusion in the glass and surface layers.

Figure 2 shows the curves having inflection points between 10th and 20th day except for Cr. The fractional release of Ba is higher than those of Na and Cs during the first 50 days, but later it decreases significantly. The release of Mg is about ten times lower than those of the other elements.

DISCUSSION

Classification of elements

The elements in the glass waste form can be classified into three groups based on time dependency of the fractional releases and the behavior of the elements in the surface layers.

Group I consists of the elements such as Na, Cs, B and Mo. The group I elements are released into water at high leach rates with the time dependency represented by $\log(FL_i) = n \log(\text{time}) + A$, which indicates that the chemical reaction in the surface layers has little influence on leach rates of these elements.

Group II consists of the elements such as Mn, Fe, Ni, Zr, Y, La, Ce, Nd, Sm and Dy. The group II elements are not detected in the leaching solution, which is consistent with their high concentration in the surface layers.

Group III consists of the elements such as Si, Ca, Al, Sr, Ba, Mg and Cr, which do not belong to group I nor group II. Time dependency of the releases of Sr, Ca and Al shows smaller deviation from linearity and these elements are released at lower rates than the elements of group I. This probably results from small amounts of these elements remained in the surface layers. Silicon may belong to this type, which we call group IIIa, because Si has the same element distribution in the layers as those of the above elements.

Barium and Mg show large deviation of the fractional release curves from linearity and high concentration in the surface layers. However, Barium has a higher leach rate, especially in the early stages, than Mg, suggesting that they may have different leaching behavior. Although Cr shows a trend of time dependency of fractional release(Fig. 2) similar to those of the group I elements(Fig. 1), it is released at a low rate and remains in the surface layers. A certain amount of Cr changes to soluble CrO_4^{-2} species[6] on the glass surface.

Leaching mechanisms

The mechanisms proposed for each group are shown in Fig. 3 schematically.

The group I elements are released into water essentially by the combination of decomposition of the glass and diffusion in the glass and the surface layers. Since these elements are depleted from the surface layers, the diffusion coefficients in the surface layers are much larger than those in the glass.

The group II elements are insoluble and do not diffuse in the glass nor in the surface layers. These elements remain in the surface layers and then form the sheet silicate.

The leaching behavior of the group III elements is different from that of group I and II but the group III elements do not necessarily show similar tendency of leaching behavior to

each other. Very small amounts of the group IIIa elements diffuse in the glass but large amounts of them leach into the solution by diffusion in the surface layers and decomposition of the glass. Some of them, however, enter the sheet silicate. The releases of Ba, Mg and Cr are controlled mainly by diffusion and the formation of the layers but the detail of its leaching behavior remains unknown.

REFERENCES

1. D. E. Clark and L. L. Hench, "An Overview of the Physical Characterization of Leached Surface," Nucl. Chem. Waste Manage., 2, 93 (1981).

2. L. L. Hench, D. E. Clark and E. L. Yen-Bower, "Corrosion of Glasses and Glass-Ceramics," Nucl. Chem. Waste Manage., 1, 59 (1980).

3. T. Murakami and T. Banba, "The Leaching Behavior of a Glass Waste Form. I: The Characteristics of Surface Layers," (in press) Nucl. Technol.

4. T. Banba and S. Tashiro, "Safety Evaluation of Simulated High-Level Waste Glass Products(I) (Thermal Stability)," JAERI-M 8706 (1980).

5. F. K. Altenhein and W. Lutze, "Long-Term Radioactivity Release form Solidified High-Level Waste - Part II: Parametric Study of Waste Form Properties, Temperature and Time," Scientific

Basis for Nuclear Waste Management VI, p. 269, D. G. Brookins, Ed., North-Holland, New York (1983).

6. B. T. Kenna, "Analysis of Long-Term Soxhlet Tests," Nucl. Chem. Waste Manage., 3, 69 (1982).

TABLE I Composition of glass waste form

Component	Content(wt%)	Component	Content(wt%)
Additive		Waste	
SiO_2	(38.3)[b]	Cr_2O_3	0.20
B_2O_3	11.8	CoO	0.09
Al_2O_3	7.38	NiO	0.42
Na_2O[a]	20.3	Ag_2O	(0.02)
K_2O	(1.14)	CdO	(0.02)
MgO	0.84	TeO_2	(0.17)
CaO	6.43	Cs_2O	0.72
TiO_2	0.09	Ce_2O_3	(1.13)
P_2O_5[a]	0.25	Nd_2O_3	(0.73)
Waste		La_2O_3	(0.35)
		Sm_2O_3	0.30
SrO	0.24	Y_2O_3	0.25
BaO	0.48	Pr_2O_3	(0.17)
Fe_2O_3[a]	4.13	Dy_2O_3	0.16
MnO_2[a]	0.22	Tb_2O_3	(0.04)
ZrO_2	1.05	Er_2O_3	(0.03)
Rb_2O	(0.10)	Gd_2O_3	(0.31)
MoO_3	1.37		

[a]Component contained in both additive and waste.

[b]Values in parentheses are calculated ones.

TABLE II Elemental fractional releases of waste glass(J-10) in Soxhlet leach test at 100°C

Time (day)	Cs	B	Mo	Na	Ba	Sr	Ca	Cr	Al	Mg
1	1.5E-2	1.3E-2	1.3E-2	1.2E-2	2.1E-2	9.0E-3	7.5E-3	5.6E-3	5.6E-3	4.0E-4
2	2.8E-2	2.4E-2	2.4E-2	2.2E-2	3.5E-2	1.6E-2	1.4E-2	1.1E-2	9.9E-3	7.5E-4
3	3.9E-2	3.3E-2	3.3E-2	3.0E-2	4.4E-2	2.2E-2	2.0E-2	1.6E-2	1.3E-2	1.0E-3
4	5.1E-2	4.3E-2	4.3E-2	3.9E-2	6.2E-2	3.0E-2	2.7E-2	2.0E-2	1.9E-2	1.4E-3
5	5.9E-2	5.2E-2	5.1E-2	4.7E-2	6.7E-2	3.4E-2	3.2E-2	2.4E-2	2.2E-2	1.7E-3
6	7.0E-2	6.2E-2	6.0E-2	5.6E-2	7.2E-2	3.9E-2	3.7E-2	2.8E-2	2.5E-2	2.0E-3
8	8.5E-2	8.0E-2	7.6E-2	7.2E-2	8.6E-2	5.0E-2	4.9E-2	3.6E-2	3.3E-2	2.7E-3
10	1.0E-1	9.7E-2	9.1E-2	8.7E-2	9.3E-2	5.9E-2	6.0E-2	4.4E-2	3.9E-2	3.2E-3
14	1.4E-1	1.3E-1	1.2E-1	1.2E-1	1.2E-1	8.3E-2	8.5E-2	5.7E-2	5.8E-2	5.3E-3
20	1.9E-1	1.7E-1	1.6E-1	1.5E-1	1.7E-1	1.3E-1	1.3E-1	7.7E-2	9.6E-2	8.1E-3
31	2.7E-1	2.3E-1	2.1E-1	2.1E-1	3.3E-1	2.1E-1	1.9E-1	1.1E-1	1.5E-1	1.2E-2
42	3.3E-1	2.9E-1	2.6E-1	2.5E-1	4.0E-1	2.5E-1	2.3E-1	1.4E-1	1.8E-1	1.3E-2
56	4.1E-1	3.5E-1	3.3E-1	3.1E-1	4.8E-1	3.1E-1	2.9E-1	1.8E-1	2.2E-1	1.6E-2
70	4.7E-1	4.1E-1	3.9E-1	3.6E-1	5.0E-1	3.6E-1	3.3E-1	2.1E-1	2.5E-1	1.9E-2
84	5.3E-1	4.6E-1	4.3E-1	4.0E-1	5.2E-1	4.0E-1	3.7E-1	2.4E-1	2.8E-1	2.1E-2
98	5.7E-1	5.1E-1	4.7E-1	4.3E-1	5.3E-1	4.2E-1	4.0E-1	2.7E-1	2.9E-1	2.2E-2
113	6.0E-1	5.5E-1	5.0E-1	4.7E-1	5.4E-1	4.6E-1	4.3E-1	2.9E-1	3.2E-1	2.4E-2
126	6.2E-1	5.8E-1	5.4E-1	5.0E-1	5.4E-1	4.8E-1	4.5E-1	3.2E-1	3.3E-1	2.4E-2
200	6.8E-1	6.8E-1	6.6E-1	6.1E-1	5.6E-1	5.5E-1	5.3E-1	4.4E-1	3.7E-1	2.6E-2

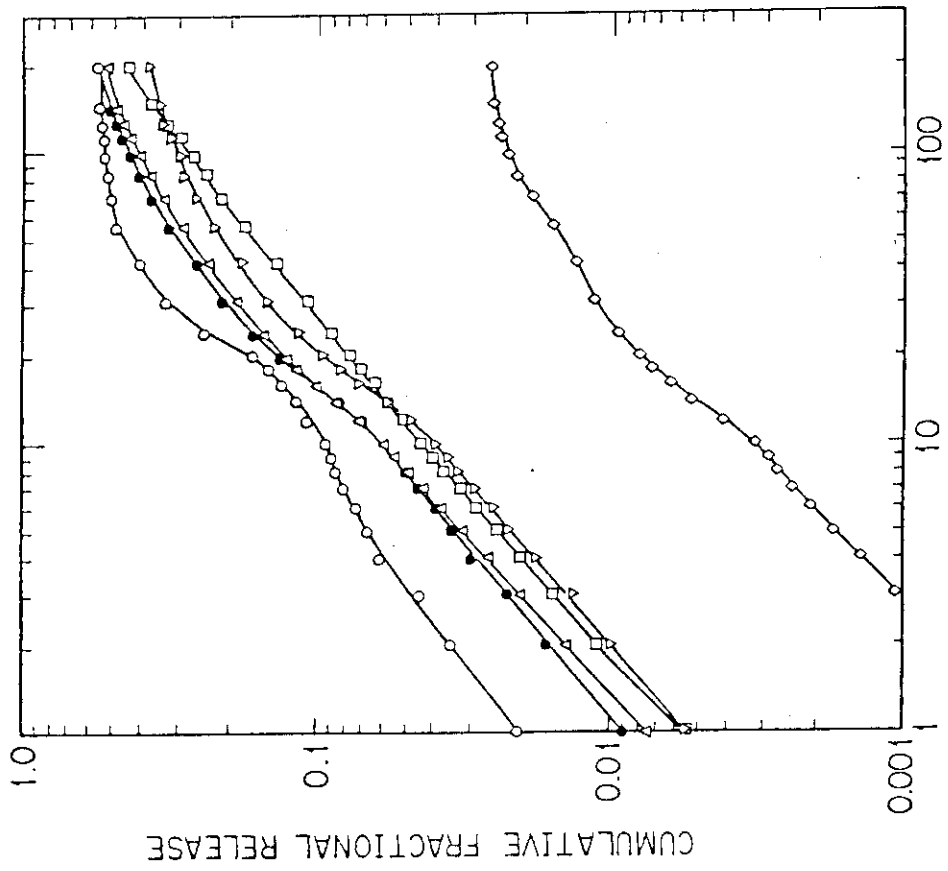

Fig. 2 Cumulative fractional releases of Ba(open circles), Sr(solid circles), Ca(triangles), Cr(squares), Al(inverse triangles) and Mg(diamonds) plotted against time for glass waste form.

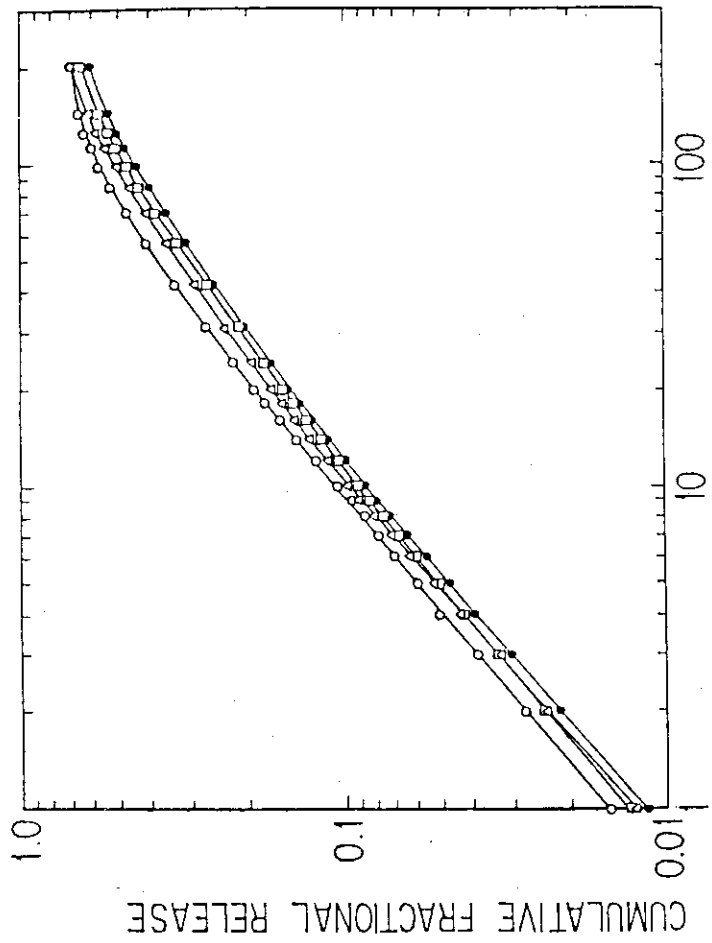

Fig. 1 Cumulative fractional releases of Cs(open circles), B(triangles), Mo(squares) and Na(solid circles) plotted against time for glass waste form.

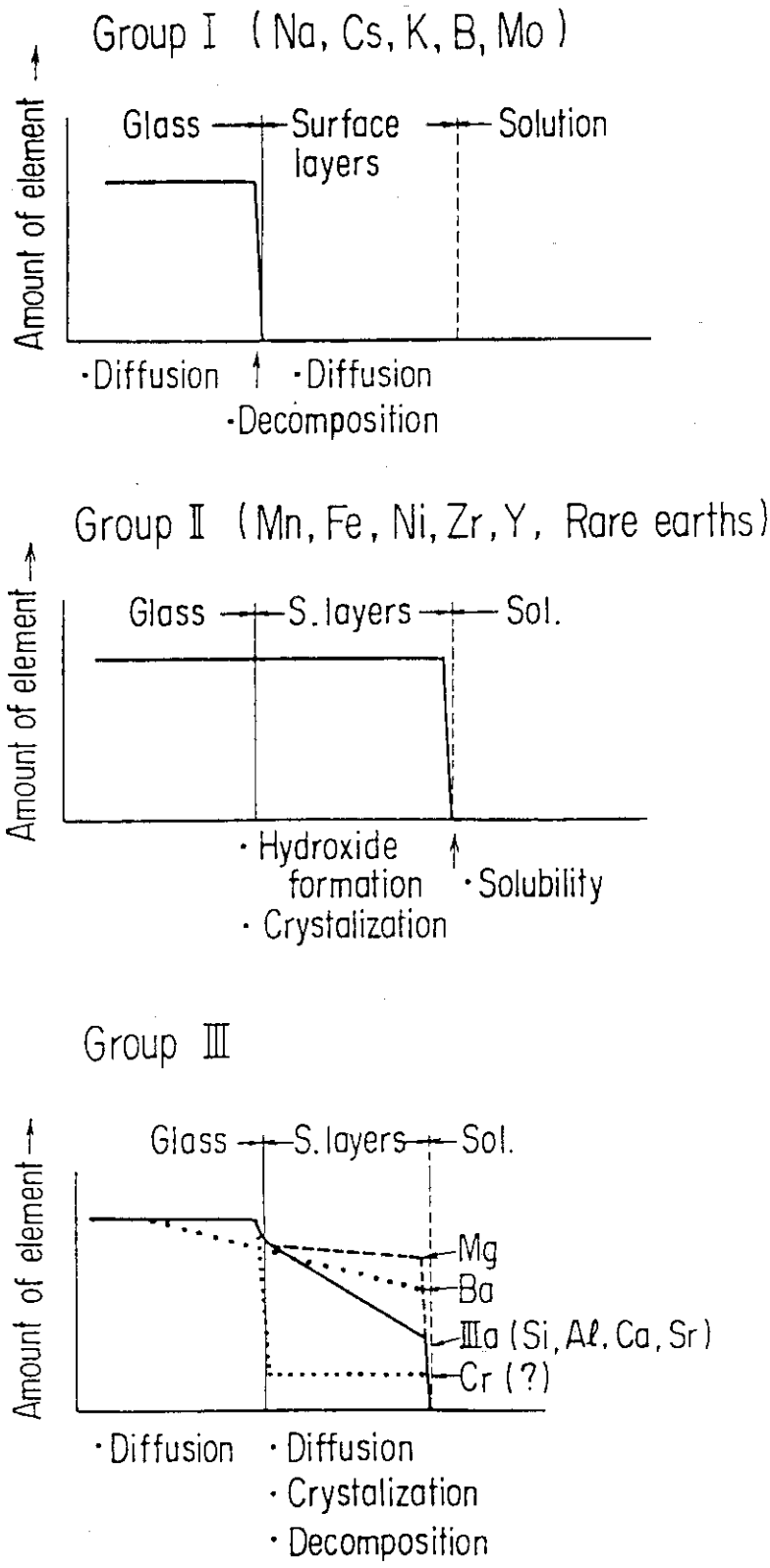

Fig. 3 Schematic diagram of leaching mechanisms of glass waste form.

1.3 Estimation of Elemental Losses of Leached Waste Glass by Surface Analysis

H. Kamizono

The first step of migration of radionuclides from the diaposal site to environmental biosphere is considered to be leaching of the radionuclides by groundwater, and so, much effort has been concentrated on the study of leaching phenomena. Solid-state analyses of leached samples along with leachate analyses are generally conducted in laboratories and provide better understanding of the mechanism of waste glass leaching.

However, the authors recently encountered two cases in which leachate analyses are difficult. One is the case in which a backfill material coexists in leachates and disturbes the exact leachate analysis due to the adsorption and dissolution of the backfill material. The other is the case in which the leach experiments are performed deep underground and the collection of leachate (groundwater) is virtually impossible. In these cases, it is necessary to get information about the extent of leaching by solid-state analyses of leached samples. The main purposes of this paper are to examine the quantitative relationship of the amount of elements on the sample surface to that in the leachate and to show that the amount of Na on the sample surface can be used as a convienient index to express the extent of leaching. In order to measure the amount of elements on the sample surface, we used scanning electron microscopy with energy dipersive X-ray analysis (SEM-EDX) for two reasons; (i) this technique provides the quantitative composition of solid-state phases quickly, (ii) with this technique, it is possible to obtain information concerning the concentration of elements up to about 5 μm below the surface of the sample.

The sample used for the present study was a borosilicate glass containing 11.7 wt% simulated high-level waste. All reagents for the simulated high-level waste were mixed with additives simultaneously, melted at 1150°C for 2 hours, poured into graphite molds, kept at 550°C for 1 hour and then slowly cooled to room temperature at a cooling rate of 20°C/hour. The resultant glass block was cut and polished into cubic specimens, which were 1 × 1 × 1 cm in size.

Static leach tests of the cubic specimens were carried out in about 20 ml of deionized water at 100°C using Teflon vessels. The duration of the leach tests was varied from 1 hour to 12 days. The SEM-EDX technique was applied to analyze the contents of elements on the surface of all

specimens. In addition, the polished section of the specimen leached for 5 days was made and elemental depth profiles were examined by the SEM-EDX technique. The accelerating voltage of electron beam was at a constant value of 20 KeV throughout the SEM-EDX observations. The concentrations of elements in leachates were measured by atomic absorption spectroscopy (AAS) and inductively coupled plasma atomic emission spectroscopy (ICP). The leachates were not concentrated before the AAS and ICP measurements. The solution pH was also monitered for each leachate at room temperature.

In order to give an example of the estimation of elemental mass losses for Na, leach tests of the simulated high-level waste glass were carried out in the presence of a backfill material. The backfill material was composed of base glass powder and bentonite powder. The cubic specimens were covered with 5 g of the backfill material and then leached in about 15 ml of deionized water at 100°C for 5 days using the Teflon vessels. The mixing ratio (G/B) of the base glass powder (G) to the bentonite powder (B) in weight was varied from 0.2 to 2. The leached specimens were then subjected to the SEM-EDX observations. The leachates were not analyzed in this case.

The results are summarized as follows;

(1) The concentration of Na on the surface of simulated high-level waste glass leached in deionized water at 100°C decreased with the duration of leach tests in days (t), following the experimental equation; $\ln C/C_0 = -0.80 \times t$, where C_0 is the concentration of Na at $t = 0$ and C is the value at t.

(2) On the other hand, the normalized elemental mass loss for Na (NL_{Na}) into leachates was changed with t as the following equation; $NL_{Na} = 3.32 \times 10^{-4} \times t^{0.80}$. The normalized elemental mass losses for Cs(NL_{Cs}) and Mo (NL_{Mo}) were almost the same as NL_{Na}.

(3) The results (1) and (2) described above gave us the following relationship of NL_{Na} to the C/C_0-value of Na;
$NL_{Na} = 3.97 \times 10^{-4} \times (-\ln C/C_0)^{0.80}$.

(4) Using the results, we reexamined the effects of a backfill material on leaching, and showed that the coexistence of the backfill material during leaching suppressed NL_{Na} by a factor of about 110.

1.4 Identification of crystalline phases in a devitrified simulated high-level waste glass containing the elements of the platinum group

H. Mitamura

Introduction

High-level radioactive waste (HLW) glasses are liable to be devitrified since HLW contains the elements of the platinum group which are hardly soluble in the glasses[1]. It is necessary to identify crystalline phases for the examination of characteristics of the devitrified HLW glasses. In the present report, crystalline phases were identified, which grew in a devitrified simulated HLW glass containing the elements of the platinum group.

Experiment

A simulated HLW glass contained 20 wt% simulated HLW oxides[2]. First, the reagents for the simulated HLW were calcined at 650 ^{0}C for 2 hours. Second, the mixture of the simulated HLW and glass additives was melted at 1200 ^{0}C for 2 hours in an alumina crucible with an electric furnace, and then it was cooled to room temperature. Third, some pieces were cut out from the central core of the crucible-shaped glass because of avoiding impurities from the pot, and then they were kept at 700

^{0}C for 1000 hours to accelerate devitrification.

Sections of the devitrified simulated HLW glass were etched by argon ion thinly enough for observation using electron microscope with energy dispersive X-ray analyzer (H-800). X-ray and electron diffraction methods were used for identification of the crystalline phases.

Results and discussion

Figure 1 shows an X-ray diffraction pattern for the powdered specimen of the devitrified simulated HLW glass. It was difficult to identify many peaks in this figure only by information from X-ray diffractometry. Elemental analyses and electron diffractometry were used for crystals in the thin specimens to facilitate identification of crystalline phases. The data of the Joint Committee on Powder Diffraction Standards were used for identification of the peaks in Figure 1.

The solid solution of ruthenium and rhodium dioxides and that of palladium, rhodium and tellurium metals were recognized, which had formed in the as-prepared simulated HLW glass.

Peaks named "A" in Figure 1 indicated the solid solution of rare earth boron silicates——$LaBSiO_5$ and $NdBSiO_5$, for example. This phase was found to be solid solution due to following facts: (1) "A" peaks in Figure 1 were slightly displaced between those of $LaBSiO_5$ and $NdBSiO_5$; (2) rare earth elements co-existed in crystals which showed electron diffraction patterns of this

phase.

Figure 2 shows transmission electron micrographs for the thin sections of the glass. Figure 3 indicated an electron diffraction pattern and an energy spectrum for one of crystals like that shown by arrow in Figure 2 (a). This phase was found to exist in a monoclinic crystal system and the state of the solid solution of rare earth phosphates——$LaPO_4$ and $NdPO_4$,for example, due to following results: (1) electron diffraction patterns like figure 3 (a) implyed that the phase was monoclinic; (2) rare earth elements co-existed in crystals which showed electron diffraction patterns like this figure. Peaks of silicon in Figure 3 (b) arose from overlapping of the glass.

Rare earth elements were also contained in the solid solution of strontium and barium molybdenum oxides, namely (Sr, Ba)MoO_4, and in an unknown phase which was rich in silicon and chromium.

Peaks named "B" in Figure 1 were those of cerium dioxide. This phase did not contain any other rare earth elements.

Figure 4 shows an electron diffraction pattern and an energy spectrum for a crystal of silicon dioxide shown by an arrow in Figure 2 (b). This phase perhaps existed in the crystalline form of cristobalite, judging from following facts: (1) Peaks named "C" in Figure 1 probably indicated the existence of cristobalite; (2) electron diffraction patterns like Figure 4 (a) also uttered the growth of this form. In my preliminary research, silicon

dioxide occurred in the crystalline form of tridymite, which grew by devitrification of a glass consisting of the glass additives and the elements of the platinum group. It may be why constituents of the simulated HLW gave the conditions to be liable to develop cristobalite.

Another unknown phase existed, which was rich in nickel and chromium.

In a future research, leaching test will be carried out to clarify leaching behavior of the devitrified simulated HLW glass.

References

(1) H. Mitamura, T, Murakami, T. Banba, Y. Kiriyama, H. Kamizono, M.Kumata and S. Tashiro, "Segregation of the elements of the platinum group in a simulated high-level waste glass", Nuclear and Chemical Waste Management (1983) (in press).

(2) Progress Report on Safety Research of High-Level Waste Management for the Period April, 1981 to May, 1982, S. Tashiro (ed.), JAERI-M 82-145 (1982).

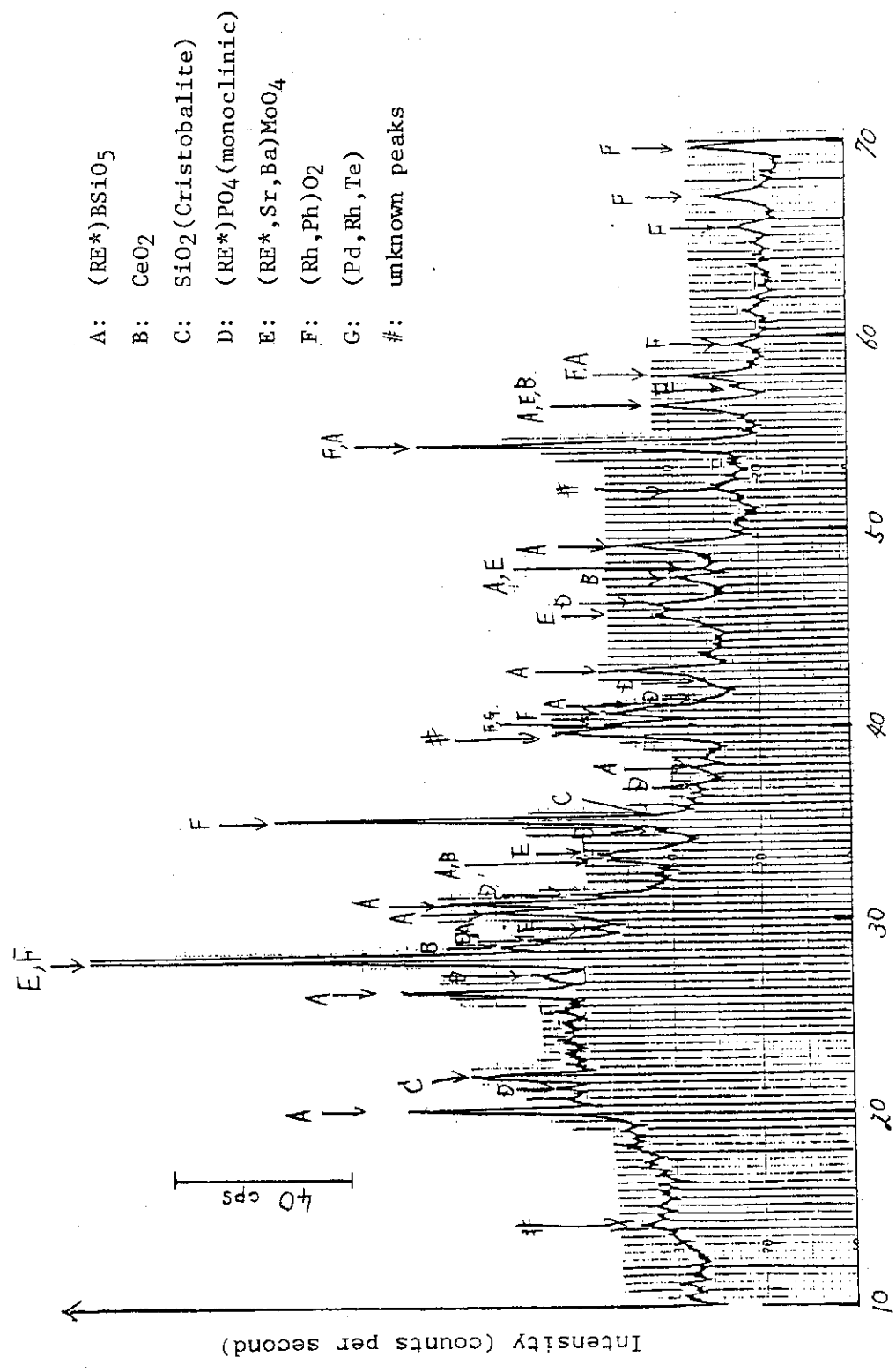

Fig. 1 X-ray diffraction pattern for the simulated high-level waste glass.
Target is copper, accelerating voltage is 35 kV and current is 15 mA.
* RE stands for rare earth elements

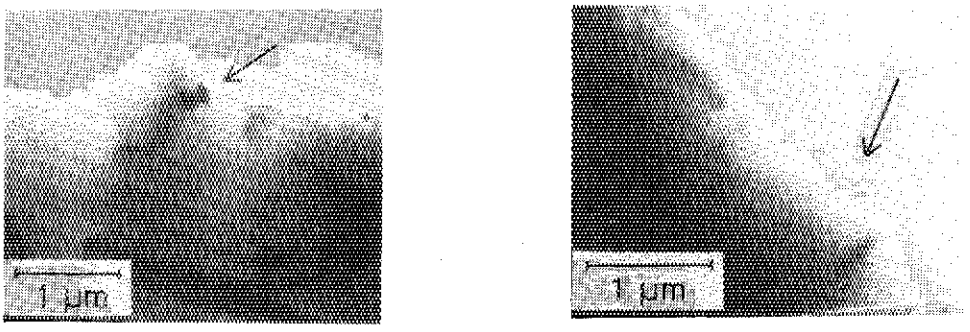

Fig. 2 Transmission electron micrographs for the devitrified simulated HLW glass. An arrow in (a) shows crystals of $(RE)PO_4$ and an arrow in (b) does that of SiO_2.

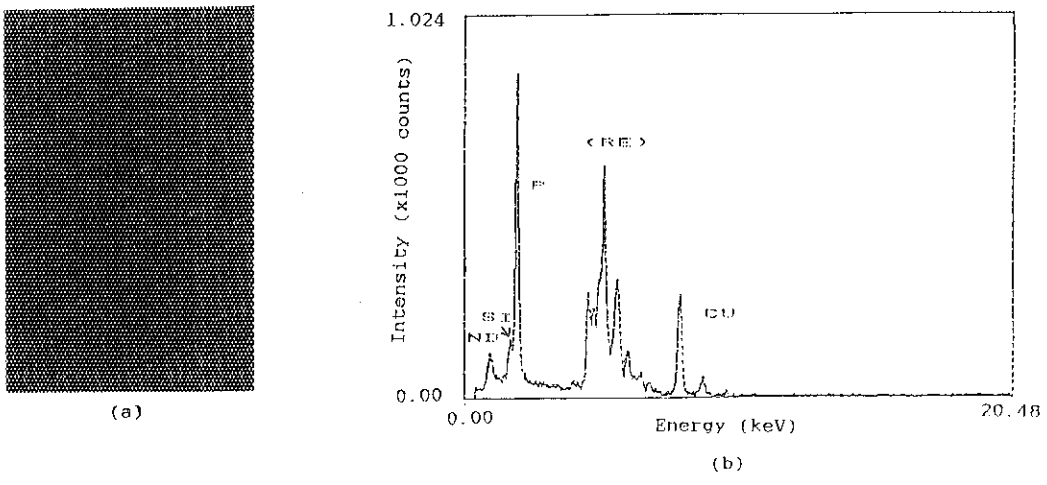

Fig. 3 Electron diffraction pattern (a) and energy spectrum with energy dispersive X-ray analysis (b) for the solid solution of rare earth phosphates. Accelerating voltage is 200 kV.

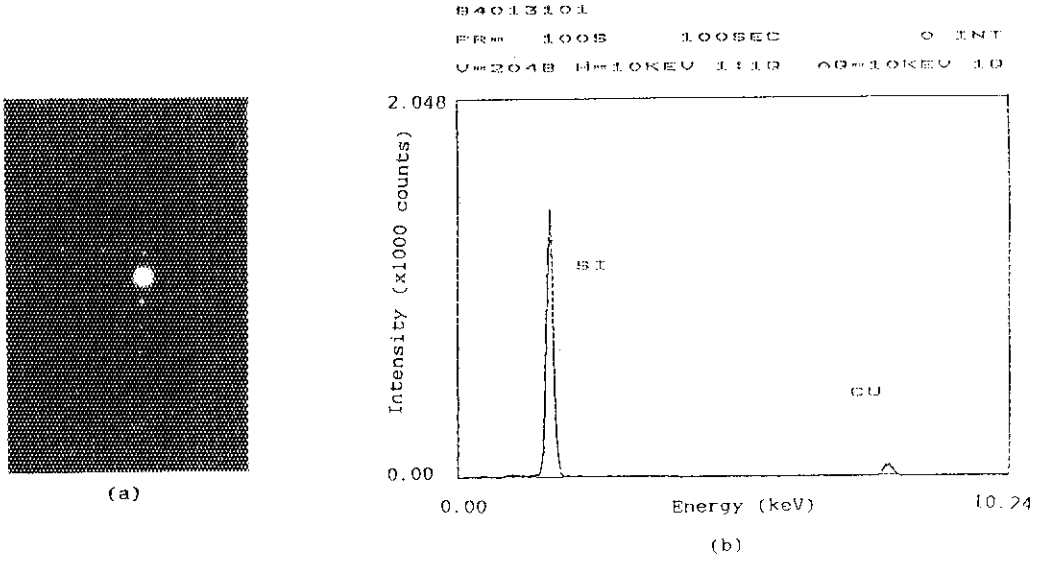

Fig. 4 Electron diffraction pattern (a) and energy spectrum with energy dispersive X-ray analysis (b) for silicon dioxide. Accelerating voltage is 200 kV.

1.5 Microstructures of SYNROC specimens synthesized by three different methods

T. Murakami

The leaching mechanisms of glass waste forms have been studied intensively because of important relevance of the mechanisms to prediction of long-term leach rates of the glass waste forms. Although the mechanisms are different between the glass and ceramic waste forms due to the different nature between glass and crystalline phases, only a few authors reported the mechanisms of the ceramic waste forms[1, 2].

On leaching of the ceramic waste forms, intergranular phases, cracks and preferentially soluble crystalline phases are considered to act as short circuit leaching paths[2] and result in rather high leach rates at the early stage of the leaching. Studies on the intergranular amorphous phases, using thin transmission electron microscope samples, revealed the preferential dissolution of the amorphous phases[3, 4, 5, 6]. Since the leaching is closely related to microstructures of the ceramic waste forms[7], it is necessary to examine and understand the microstructures of the ceramic waste forms including grain size, distribution of the major and minor phases and distribution of radioactive waste elements among the phases.

Since the SYNROC waste form[8] is one of the most feasible

alternatives[9], microstructure of SYNROC[7, 8, 10, 11, 12, 13] should be examined to elucidate the leaching mechanisms of SYNROC. In the present study, texture and distribution of waste elements are discussed using three SYNROC samples synthesized with three different synthesizing methods.

Experimental

The composition of SYNROC is given in Table 1. The SYNROC specimens were synthesized containing 10 wt% nonradioactive simulated high level wastes[13] and 90 wt% additives, and expected to consist of 33 wt% perovskite, 35 wt% hollandite and 32 wt% zirconolite. Nonradioactive simulated wastes were added as nitrates, except for Ru, Pd, Mo and Te which were used in the forms of RuO_2, PdO, $H_2MoO_4H_2O$ and TeO, respectively. The additives were composed of titania, zirconia, alumina and Ba- and Ca- nitrates.

The fabrication procedure was as follows: 1. The nonradioactive simulated wastes and the additives were mixed by ballmilling in ethyl alcohol for 21 hours. 2. The mixture was calcined at 700°C for 4 hours and then 1000°C for 16 hours in nitrogen gaseous atmosphere. 3. Titanium metal powder was added to the calcined powder and they were mixed by ballmilling for 17 hours. 4. The final mixture was divided into three, which were subjected to the three different synthesizing methods,

respectively; HUP (hot uniaxial pressing), HIP (hot isostatic pressing) and AS (atmospheric sintering). The conditions for HUP were at 1200°C and 600 kg/cm^2 for 3 hours in nitrogen gaseous atmosphere, those for HIP were at 1200°C and 800 kg/cm^2 for one hour in argon gaseous atmosphere, and those for AS were at 1300°C for 26 hours in air.

The major phases of the HUP, HIP and AS specimens were identified by X-ray diffractometry. The textures of the major and the minor phases and distribution of waste elements were observed and analyzed with transmission electron micrscope (TEM) and scanning electron microscope (SEM) both equiped with energy dispersive X-ray spectroscopes (EDX). The samples for TEM were prepared by ion beam thinning using argon ions.

Results and discussion

Figures 1(A), 1(B) and 1(C) show the X-ray diffractograms of HUP, HIP and AS specimens, respectively. The X-ray diffractogram of the calcined mixture before synthesis is also given for comparison. Besides the three phases, hollandite, perovskite and ziconolite, magnetoplumbite (labelled M in Fig. 1) also formed in the HUP, HIP and AS specimens. Some amounts of rutile remained without reaction in the AS specimen. Metal phases were not detected by X-ray diffractometry.

Figures 2 and 3 show the transmission electron micrographs

of the HUP and HIP specimens, respectively which indicate similarity of microstructures of the two specimens. The two specimens have very compact structure in which the grain sizes of crystals (hollandite, perovskite and zirconolite) are less than 1 micrometer in diameter. Small metal phases are observed mainly in grain boundaries as shown by arrows.

The AS microstructure has different aspect from those of HUP and HIP (Fig. 4). Crystals have large grain sizes from 1 to 20 micrometers and few metal phases are observed. The most distinguished feature of the AS microstructure is that apparent glass phases form (arrows in Fig. 4) which contain Mo and Cs. Elemental analyses revealed that the other phases of the AS specimen do not contain Mo of Cs except only small amounts of Mo in perovskite and metal.

Although apparent glass phases cannot be observed in the micrographs of the HUP and HIP specimens, the amorphous halos in Fig. 5 indicate that there exist glass phases between grain boundaries also in the HUP and HIP specimens. However, smaller amounts of Mo and Cs, if any, are contained by the glass phases in the HUP and HIP specimens than in the AS specimen because elemental analyses indicated most of Mo and Cs enter metal phases and hollandite respectively in the HUP and HIP specimens.

The relationships between the mictrostructures and the leach rates are now investigated.

References

1. Ryerson, F. J., Bazan, F., Campbell, J. H.; J.Amer. Ceram. Soc., 66, 462 (1983)
2. Clarke, D. R. and Flintoff, J. F.; Sci. Bas., 6, 29 (1983)
3. Clarke, D. R.; J. Amer. Ceram. Soc., 64, C-89 (1981)
4. Clarke, D. R., Jantzen, C. M., Harker, A. B.; Nucl. Chem. Waste Manag., 3, 59 (1982)
5. Dosch, R. G.; Sci. Bas., 4, 15 (1982)
6. Sethi, V. K., Bates, J. K.; Nucl. Technol., 60,228 (1983)
7. Cousens, D. R. et al.; Sci. Bas., 5, 309 (1982)
8. Ringwood, A. E. et al.; Geochem. J., 13, 141 (1979)
9. Ringwood, A. E., Major, A., Ramm, E. J., Padgett, J.; Nucl. Chem. Waste Manag., 4, 135 (1983)
10. Reeve, K. D. et al.; in Proceedings of the Symposium on Waste Management at Tucson, Arizona (1981)
11. Ryerson, F. J., Hoenig, C. L., Smith, G. S.; UCRL-86880 (1981)
12. Murakami, T.; Mineral. J., 11, 344 (1983)
13. Banba, T. et al.; JAERI-M 82-088 (1982)

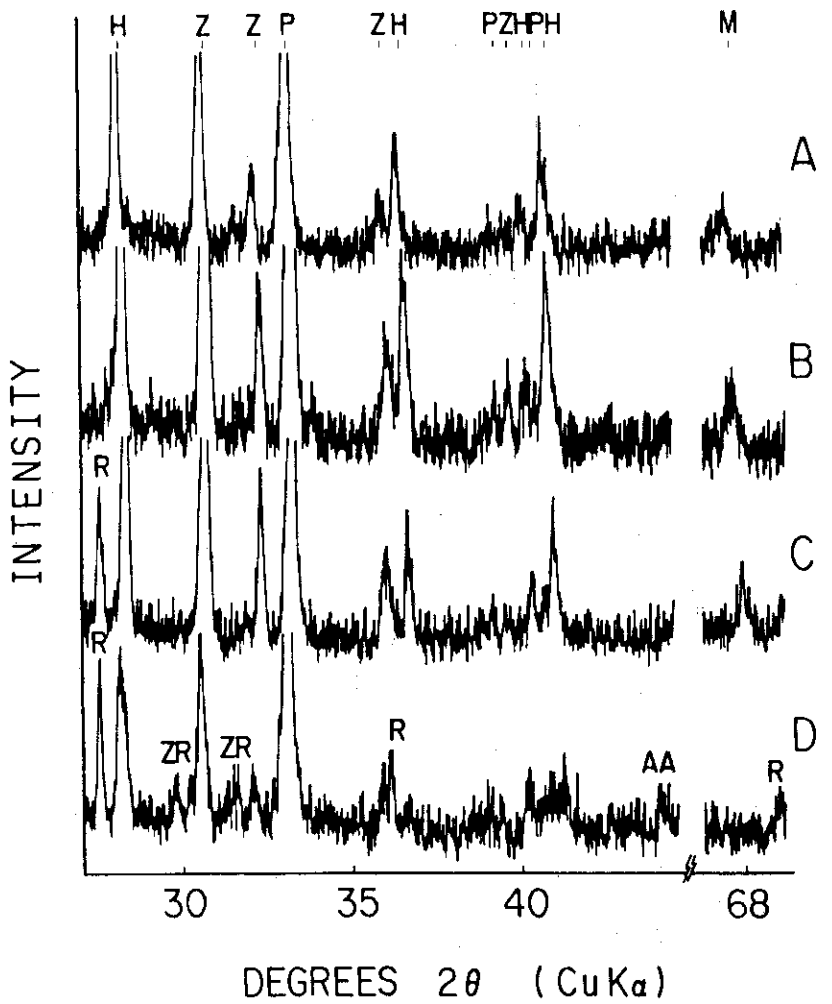

Fig. 1 X-ray diagrams for A; HUP, B; HIP, C; AS and D; calcined mixture before synthesis. H; hollandite, P; perovskite, Z; zirconolite, M; magnetoplumbite, R; rutile, ZR; zirconia and AA; alpha-alumina.

Additives			
TiO_2	55.41	Al_2O_3	4.03
CaO	13.48	BaO	6.20
ZrO_2	9.08	Ti	2.00
Wastes			
RuO_2	0.58	PdO	0.33
SrO	0.18	MoO_3	0.92
MnO_2	0.14	TeO_2	0.12
Cs_2O	0.52	Pr_6O_{11}	1.31
Nd_2O_3	1.21	Na_2O	1.69
Fe_2O_3	1.42	Cr_2O_3	0.21
NiO	0.18	ZrO_2	0.87
BaO	0.33		

Table 1 Composition of SYNROC specimens

Fig. 2 Transmission electron micrograph for HUP. A bar indicates 1 micrometer. Arrows show examples of metal phases.

Fig. 3 Transmission electron micrograph for HIP. A bar indicates 1 micrometer. Arrows show examples of metal phases.

Fig. 4 Transmission electron micrograph for AS. A bar indicates 1 micrometer. Arrows accompanied by G show the locations of glass phases.

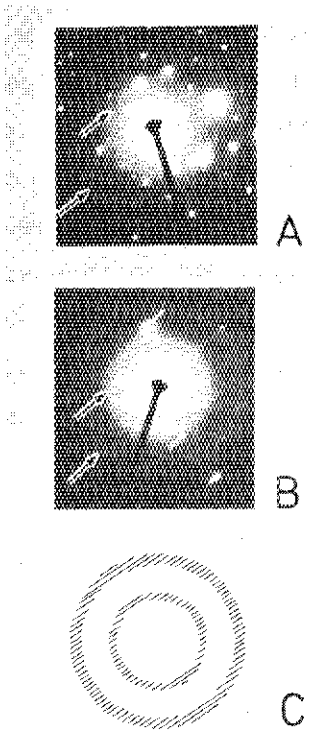

Fig. 5 Electron diffraction of amorphous halos for A; HUP, B; HIP and C; schematic diagram. Arrows indicate the location of amorphous halos.

2. Safety evaluation of geologic disposal

S. Muraoka

Information regarding characteristics of underground rock mass are indispensable to assess the safety of geologic disposal of high level waste. In this fiscal year, accumulation of data for safety assessments was initiated in cooperation with constructors of underground facilities. Some of general phenomena such as the relation between permeability and depth, and abundance of fracture healed with secondary minerals were investigated.

The underground experiments in a metal mine were continued and a new facility was constructed in a granite rock mass at near surface. Fundamental experiments regarding thermal effects on rock mass characteristics, performance of artificial barrier and ground water behavior will be carried out.

The durability tests of near field barrier materials were continued under γ-ray irradiation in WASTEF and JMTR. A system performance tests using high pressure vessel were started in this fiscal year. As the first stage, heat conductivity was measured with 1/5 scale model simulating the arrangement of repository bore hole.

In order to define the place, where water is sunk and nuclides are mineralized, diffusion test of various nuclides were carried out by using small rock samples. The result shows porosity was important for the distribution of nuclides in rock samples.

In the development of nuclide migration code 3 dimensional seepage flow code with modified double porosity model was developed to assess the water flow in rock mass containing fracture.

2.1 Field survey

2.1.1 Accumulation of informations regarding characteristics of deep underground rock mass from construction work of underground facilities

H. Nakamura

General informations regarding characteristics of deep underground rock mass are indispensable to assess the safety of geological disposal of high level waste especially on a stage of no candidate disposal site. Informations from construction work of underground facilities at various sites are collected and analyzed. Data from granite sites were analyzed in this year, which show rare site dependency and simple rock mass formation.

1. Relation between permeability and depth

Permeability measured in bore holes were plotted against the depth in Fig. 1. Maximum permeability at each depth decreased linearly with depth by a ratio of 1/10 for 100 m approximately.

Initial stresses were measured using a acoustic emission (AE) instrumentation system for core samples gathered from granitic rock areas. The results showed that the pressures correspond to a column pressure of rock.

Increasing of the pressure with the depth causes the reduction of the permeability by closing fractures.

2. Ratio of fractures healed with secondary minerals originated from rock weathering

Typical minerals filling fractures were epidote, quartz, calcite and chlorite. Calcite and chlorite possibly originated from rock weathering. The sum of fractures healed with calcite and chlorite were plotted in Fig. 2 against number of total fractures per 10m. The fractures healed with them increase with total fracture abundance. Almost all the fractures were healed with them at places of fracture abundances of 100 per 10m, while only 10% of them were healed at places of that 10 for 10m.

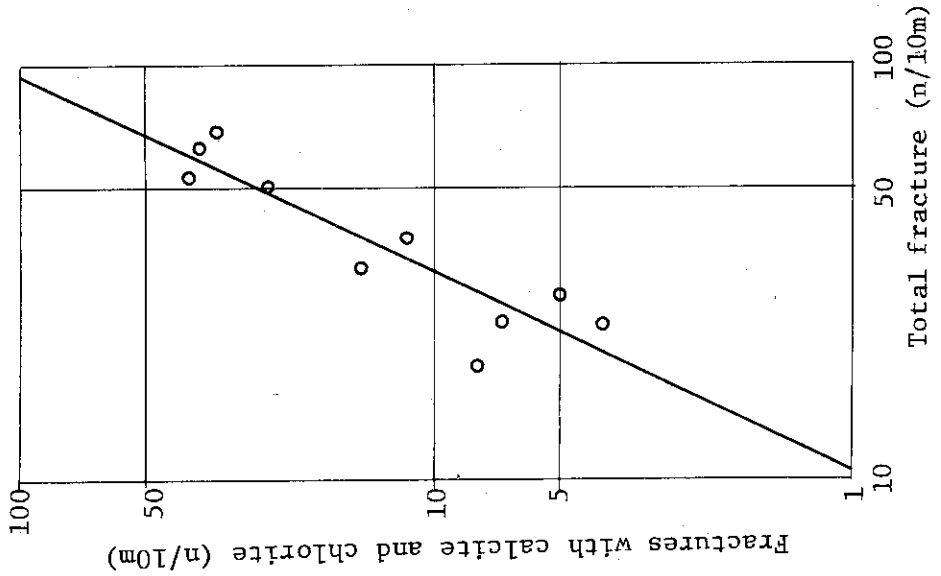

Fig. 2 Abundance of fractures with calcite and chlorite

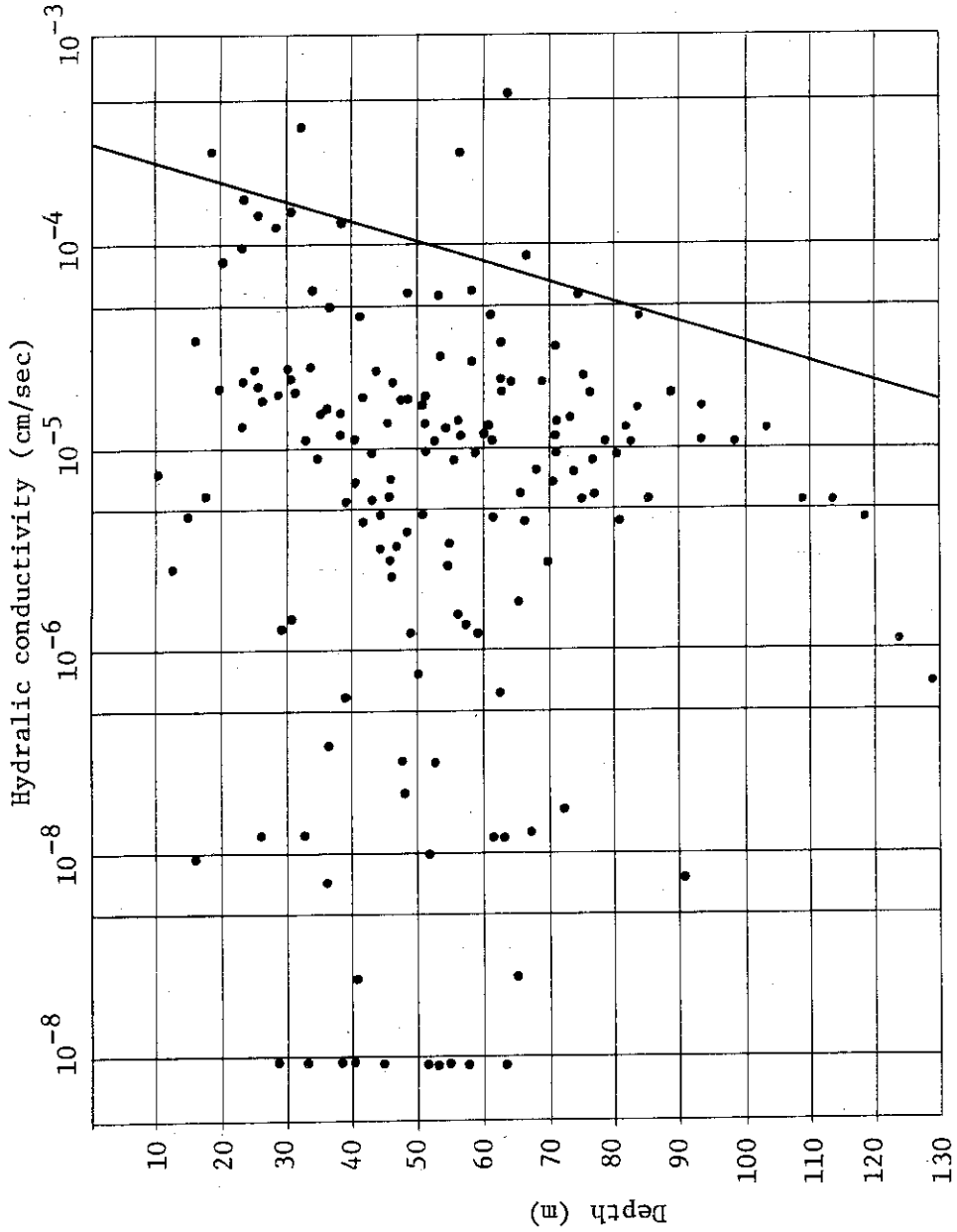

Fig. 1 Relation between permeability and depth

2.1.2 Study on the behaviour of radium in natural rocks

M. Kumata and H. Nakamura

For the safety assessment of the geological disposal of the high-level radioactive waste (HLW), it is very important to predict a radionuclide migration of HLW elements released from a repository in deep geological environments. Natural analogue is a persuasive approach for long term safety assessment of geological disposal. Behaviour of radioactive materials in a hot spring was investigated as one of natural analogue of nuclides migration. Several specimens were sampled from the Masutomi hot spring, which is one of famous radioactive mineral spring in Japan, and from the Hontani river near the spring.

1. Distribution of activities in rock

A large granite rock specimen sampled from the Togetsu-ann was investigated in detail. Radioactivities of brown precipitate and rock in the spring were measured by gas flow type proportional counter. Fine powder of these samples were prepared for the alpha-ray measurement by grinding and 2g of the powder was taken on stainless steel dish of 1 inch dia. The samples were thick enough against the range of alpha particles.

The result is shown in Table 1. The radioactivities were concentrated in the precipitate which is the sinter of the mineral spring. The concentration of radioactivity of rock was

only a few per cent of the value of the precipitate.

A core was taken from the rock specimen of about 15 cm thick, which was sunk in the mineral spring for long time. The distribution of radioactivity of the core showed no meaningfull activity gradient with the depth.

Compositions of rock and precipitate were measured by X-ray fluorescence analysis. The results shown in Table 2 shows that iron is concentrated in precipitate, where no crystalized minerals were detected by X-ray diffraction analysis.

2. Gamma-ray spectrometry

Sampled rock specimens from the Masutomi mineral spring and the Hontani river were almost weathered granite. For these samples, gamma-ray spectrometry was performed by means of a high pure Ge semiconductor detector with multi-channel analyzer.

The natural radioactive decay series include four isotopes of radium ; ^{226}Ra (half-life=1600yr) in the uranium series, ^{223}Ra (half-life=11.4days) in the actinium series, and ^{228}Ra (half-life=5.8yr) and ^{224}Ra (half-life=3.64days) in the thorium series.

Gamma-ray spectra of samples showed almost same patern. Fig.1 shows the gamma ray spectrum of the precipitated brown material and rock specimen sampled from the Masutomi spring. These spectra were decided to ^{208}Tl, ^{212}Pb, ^{212}Bi, ^{214}Pb, ^{214}Bi, ^{228}Ac and ^{40}K. ^{40}K is characteristic of natural rocks. ^{214}Pb and ^{214}Bi are daughter nuclides of ^{226}Ra and named RaB and RaC

respectively. ^{228}Ac, ^{212}Pb, ^{212}Bi and ^{208}Tl are daughter nuclides of ^{228}Ra in the thorium series.

In order to compare the spectra of these samples and other granite, gamma-ray spectrometry was performed for the Inada granite. The spectra of the Inada granite were also similar to the other ones.

Table 1 Alpha activity contained in rock

Precipitate	19,558 cph
Stone	404 cph

Table 2 X-ray fluorescence analysis of sampled rock and precipitate

Component	rock(wt%)	precipitate(wt%)
SiO_2	77.36	41.13
Al_2O_3	12.24	5.35
Fe_2O_3	1.63	28.53
CaO	0.61	8.88
Na_2O	3.40	1.02
TiO_2	0.05	0.09
MnO	0.02	0.12
P_2O_5	0.01	0.01
Total	95.32	85.13

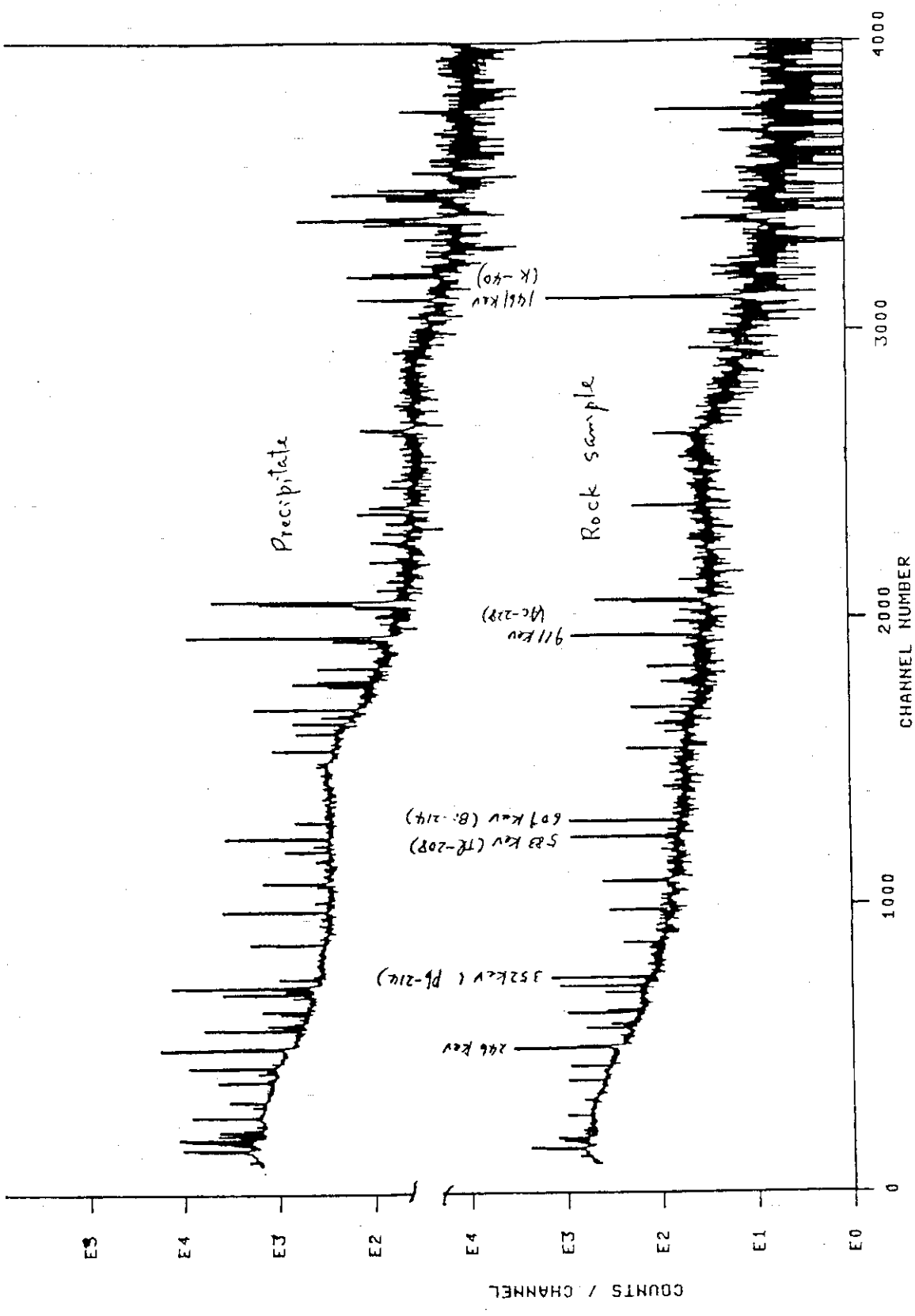

Fig. 1 γ-ray spectrum of mimerals in a hot spring

2.2 In-situ experiments

M. Kumata

INTRODUCTION

The Japan Atomic Energy Commission announced guidelines for radioactive waste management in 1976. The time schedule for these guidelines was established in 1980 for high-level waste (HLW) management.

For the safety assessment on deep geological disposal for HLW, it is necessary to know the geological, geochemical, geophsical and hydrological conditions of a underground repository. In order to predict the behaviour of hard rocks and nuclides migration in circumstances that would exist in a radioactive waste repository, it is necessary to perform in-situ experiments and measurements at similar depth to that of the repository.

Japan Atomic Energy Research Institute (JAERI) performed to develop the measurement technique, instruments and analytical methods concerning in-situ experiments. The drift at the depth of 380m under the earth surface in the Akenobe mine in southwest Japan was used for the in-situ experiments. The rock type was shalstein of Permian age.

HEATER TEST

For the research of the heat transfer in the rock mass and the mechanical behaviour of rock under thermal stress, field

tests have been conducted since the end of 1977 [1]. The temperature and thermal stress distributions have been investigated using two electrical heaters to simulate the heat of vitrified HLW. Also, the behaviour of water which are contained in rock mass around the heater was investigated (Figure 1-1).

The heaters were composed of nichrom wire surrounded by magnesia insulation and sheathed with stainless steel tube. The dimension was 2.2 m in length and 25.4 mm in outer diameter. Two 29 mm diameter boreholes were drilled for the heaters and seven boreholes (the same diameter) were for thermocouples. The boreholes were horizontal and approximately 7.5 m deep from the wall-rock surface. The heaters were separated from each other in such a way that each heater simulates a single canister emplacement. The electric power of the heaters were kept constant at around 2kW for first 47 days, and after 26 days cooling the power was raised to 4kW and kept for further 48 days. Temperatures were measured by the twenty chromel-alumel thermocouples which were placed in each boreholes. The accuracy of temperature measurment was within 0.1°C. Comparing the observed temperature with calculated one, effects of vaporization of water in the rock mass was clearly observed. Partly, the observed temperature agreed with calculated one using the core sample's thermal conductivity, 2.9 W/m°C.

The thermal stress of rock mass was measured by strain gauges and strain meters. The thermally induced stresses has

been measured by using six rosette gauses with dummy gauges on the wall-rock surface and two mold gauges in a horizontal borehole.

For the research of thermal effect on permeability of rock, the double packer method was used to measure permeability of a rock mass around the heater. Measurements were performed for three times: before heaters on, at elevated temperature and after cooling. The distance between two rubber packers was set to be 45 cm and water was supplied with a pressure of 3, 6, 10 and 18 kg/cm^2.

MIGRATION TEST

Retardation of the migration of radioactive nuclides is due to the sorption of ions on minerals, not only in rock but also in fractures. Importance of in-situ test is that natural and real structure of a fracture is only available. The experiment was carried out at the same site used for heat conductivity test. Double packers were inserted in a hole at about 18cm and 68cm in depth from the wall-rock surface (Figure 1-2). The solution, including nonradioactive elements as tracers, was charged into the borehole at 4 kg/cm^2 pressure by compressor. LiI, $CsNO_3$, $Ba(NO_3)_2$, $Sr(NO_3)_2$ and $ZrO(NO_3)_2$ were dissolved in water to prepare the solutions of 50 - 100 $\mu g/ml$ of metal elements.

Typical break through curves are shown in Figure 2.

BUFFER MASS TEST

Buffer material is expected to play an important role as an engineered barrier in a multi-barrier system of geological disposal of HLW. Thermal conductivity and water content change of bentonite were measured. The experimental vertical hole was drilled to 330 mm in radius and 3.3 m in depth. After drilling, several fissures were observed on the inner wall of the hole and the water seepage was found at three parts of these fissures. In this hole KUNIGEL VA Bentonite, almost Na-montmorillonite, was solidified by use of 20 ton oil pressure jack with a pressure of 20 kg/cm^2. An electric heater and thermocouples were emplaced in such a geometry as shown in Figure 1-3.

Measurments of the water content change of the buffer mass was carried out used neutron scatter method with ^{252}Cf, before the heater power on and after power off.

These experiments finished in May 1984 and a part of the results was already published [2].

FUTURE EXPERIMENTS

More systematical experiments of in-situ test is designed at a new site of granite rock mass. A new underground laboratory has been constructed at the near surface for an exclusive use on safety research for geological disposal of HLW. Excavation of a gallery and test room were already finished. A microcomputer

system would be used for data logging. A borehole television set would be also used for direct observation of fractures in a borehole. Heater test, migration test and system performance test are planned at the labolatory.

REFERENCES

[1] Araki, K. et al. : "Preliminary Research on Geological Isolation of High-level Radioactive Waste at the Japan Atomic Energy Research Institute" Proc. Symp. Underground Disposea of Radioactive Waste, Finland (1979).

[2] Shimooka, K. et al. : "Pilot Research Projects for Underground Disposal of Radioactive Waste in Japan" Proc. Conf. Radioactive Waste Management, Seattle (1983).

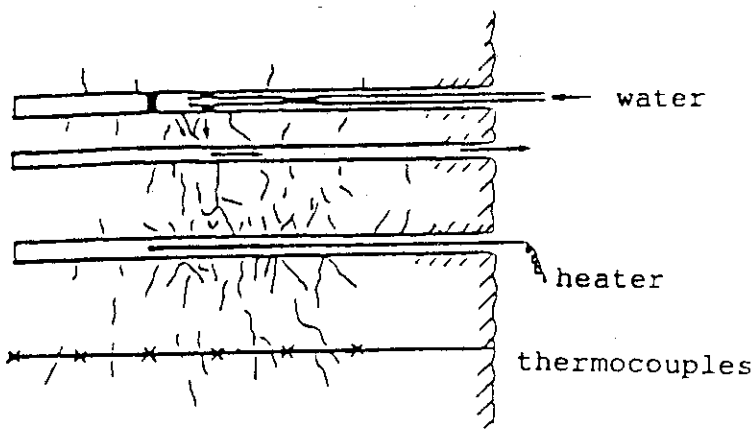

Figure 1-1 Heater Experiment

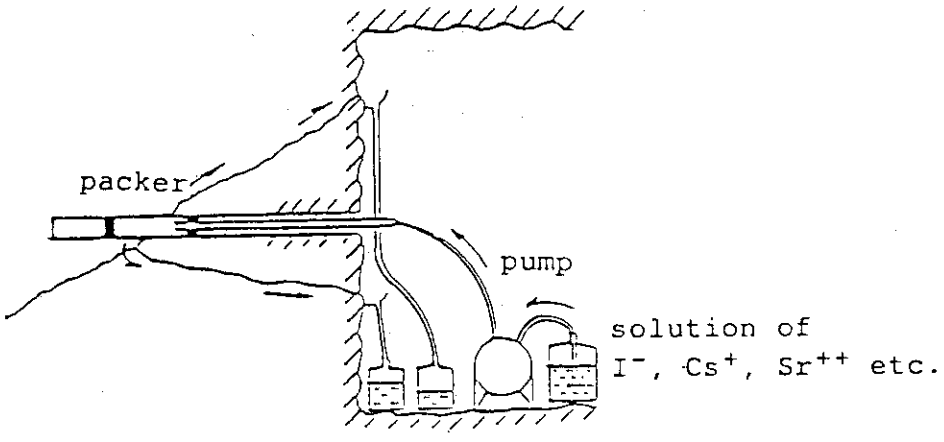

Figure 1-2 Migration Test

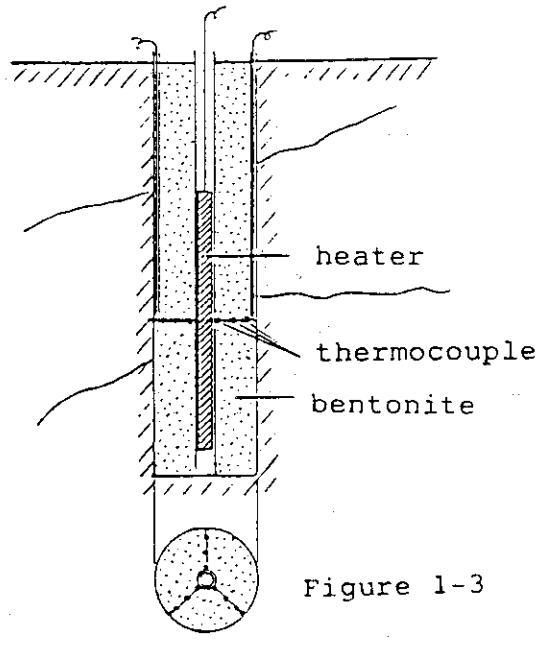

Figure 1-3 Buffer Mass Test

Fig. 1 Conceptual design of in-situ experiments at Akenobe mine

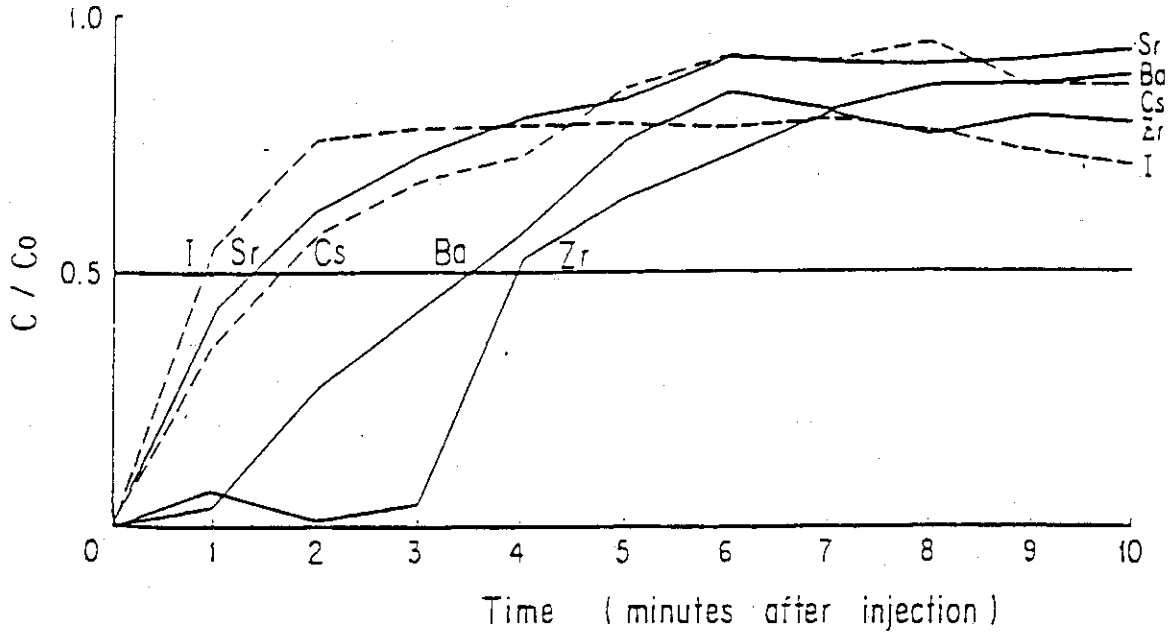

Fig. 2 Concentration curve for the fracture flow path

2.3 Laboratory tests

2.3.1 Stress corrosion cracking of austenitic stainless steels in simulated disposal environment

S. Muraoka

Introduction

In the safety assessment of the storage and geological disposal of high level waste, corrosion resistance of the canister material must be evaluated. Among many candidates, stainless steel, Ti and Ticode are thought to be promissing now. Type 309s stainless steel is a candidate of canister material for waste to be returned from over-sea reprocessing. Stress corrosion cracking of austenitic stainless steel were found in the reactor material in 1960's and have been studied under neutron irradiation. There are few study about stress corrosion cracking under gamma-rays irradiation and at low temperature. In order to elucidate the effect of gamma-rays irradiation on the stress corrosion cracking of austenitic stainless steel, irradiation corrosion test has been carried in WASTEF and in JMTR.

Experimental

Chemical composition and heat treatment of the stainless steels used in the experiments are listed in Table 1. Double U bent specimens of 1 mm thickness for stress corrosion cracking test were encapsuled in stainless steel made capsule with granite block and simulated ground water. Gamma-rays irradiation tests were carried out by use of two types of gamma-rays source. One is Cs of 2660 Ci and another is JMTR spent fuel. Schematic arrangement of each test are shown in Fig. 1. Table 2 shows the experimental condition. Susceptibity of stress corrosion cracking for the specimen were evaluated by surface and section observation with optical microscope. The fractured surface was also examined with scanning electron microscopy.

The solution were analyzed for their change between before and after tests by AAS and ICP.

Results and discussion

Experimental results from all the tests are summarized in Table 3. Type 304 stainless steel appeared to be sensitive to SCC at the dose of

1.4×10^{9}R in deionized water and at the dose of 4.1×10^{9}R in simulated ground water. On the other hand Type 390s stainless steel showed resistance to SCC in the dose range of 1.2×10^{8}-4.1×10^{9}R. This difference might be attributed to the difference of Cr and Ni contents in these steels. No cracks were observed in the both steel without gamma-rays irradiation. All cracks propagated intergranularly as shown in Fig. 2.

After irradiation tests which showed SCC and crevice corrosion, the quantity of solution decreased. The brown precipitates were observed after irradiation of 6.6×10^{8} to 1.4×10^{9}R in simulated ground water. The delay of SCC in simulated ground water in comparison with deionized water was thought to be due to the leachant from rock sample.

The value of pH increased in proportion to the dose. This might be due to the H^{+} ion increase resulted from the reaction between stainless steel with oxidizing agents produced by radiolysis of solution.

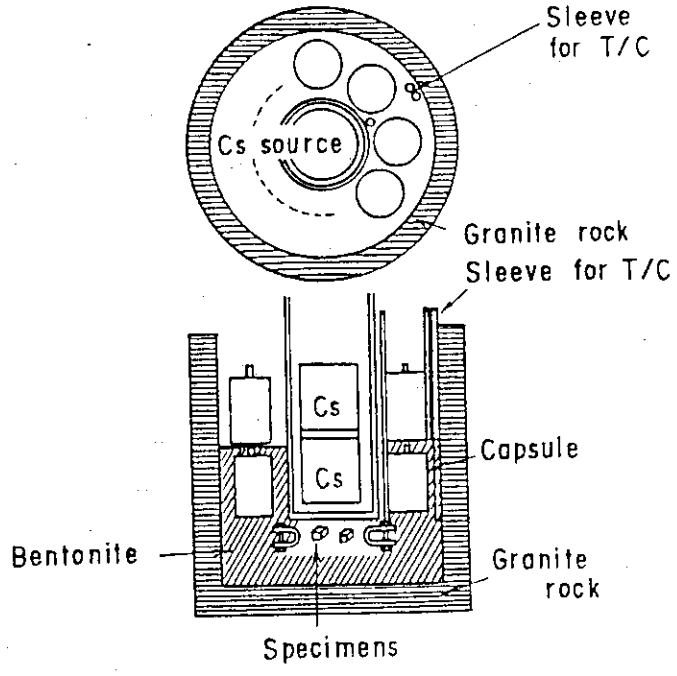

Fig. 1 Arrangement of the specimen around Cs source

Table 1 Chemical composition and heat treatment of test materials

Alloy	Composition (%)							Heat treatment
	C	Si	Mn	P	S	Ni	Cr	
Type 304 ss	0.075	0.52	0.95	0.010	0.024	9.2	18.22	700°C x 100 min. → 500°C x 24 hr. → Air cooling
Type 309S ss	0.14	0.56	1.53	0.023	<0.005	14.30	23.76	1050°C x 30 min → 700°C x 100 min → 500°C x 24 hr → Air cooling

+ Balance : Fe

Table 2 Experimental condition

		Temp.(°C)	Dose rate($\times 10^6$R/h)	Time($\times 10^3$hr)	Dose($\times 10^9$R)
Cs	I	48	0.3	2.2	0.66
	II			4.5	1.4
Spent fuel	I	21 - 52	0.35 - 5.9	6.2	4.1
	II	23 - 38	1.5 - 3.4	0.65	1.1
	III	19	0.12 - 0.26	0.65	0.12
Cold		50	——	5.4	——

Table 3 Experimental Results

	Dose ($\times 10^9$ R)	Failure	pH
Pure water	0.12	○	5.0
	0.66	○	5.5
	1.1	○	3.3
	1.4	◑ ●	3.1 / 6.4
	4.1	◑	2.6
(cold)	–	○	6.2
Simulated ground water	0.12	○	6.1
	0.66	○	5.9
	1.1	○	6.0
	1.4	○	6.3
	4.1	◑ ●	7.0 / 9.0
(cold)	–	○	7.0

Initial pH : Pure water 5.6
Simulated ground water 7.7

● : SCC

◑ : Crevice Corrosion

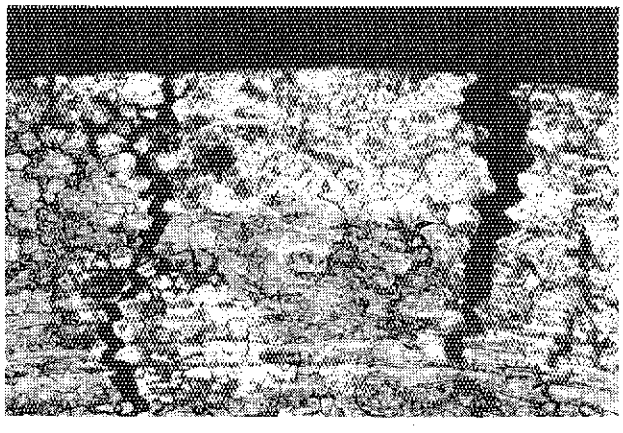

(x 100)

Fig. 3 SCC modes in Type 304 SS specimen

2.3.2 System performance tests of very near field under high pressure condition

T. Yanagida

Introduction

The canister containing vitrified high level waste will be disposed in deep geolocal formations. After sealing the repository site may be loaded with high pressure caused by rock mass and water head. System performance tests of very near field configuration by using high pressure vessel are started. As the first stage of the test the heat conductivity of buffer materials was measured in the arrangement of repository bore hole of 1/5 scale simulation. A electrical heater was used to simulate heat generation from high level waste glass.

Experimental

The buffer material used in this experiment was Na-bentonite (KUNIGELVA), and a container simulating the host rock was made of granite (INADA granite). The granite container was stuffed with bentonite of which water content was about 150 weight percent and the heater was set in the center of bentonite cylinder. Eight thermocouples were arranged around the heater, 6 in the bentonite and 2 on the outer surface of the granite container. Fig. 1 shows the conceptual layout of this experiment. The apparatus were settled in the high pressure water vessel and were pressurized through the medium of water at 50, 100 and 200 kg/cm^2. Under each pressure, heater temperature was kept at 100 and 200°C for over 24 hours.

When the system was stationary, temperature distribution was measured under each pressure, at each temperature.

Results

Fig. 2, shows the temperature distribution in bentonite and granite under pressures of 200 kg/cm^2.

Generally, the temperature distribution of this case is expressed in the following equation.

$$t1 - t = q \ln(r/r1) / 2\pi K 1$$

t1 : temperature at base point, °C

t : temperature, °C

q : quantity of heat, Kcal/h
K : thermal conductivity, Kcal/m·h°C
l : length, m
rl : radius at base point, m
r : radius, m

K values versus pressure at 100°C of heater surface is shown in Fig. 3.
In bentonite, K values slightly increase with rising pressure.
This result suggests that increasing density of bentonite caused of rising pressure influences on K value.
On the other hand, the apparent K values decrease with rising pressure in granite.
The K value of bentonite is ten times larger than that of granite.

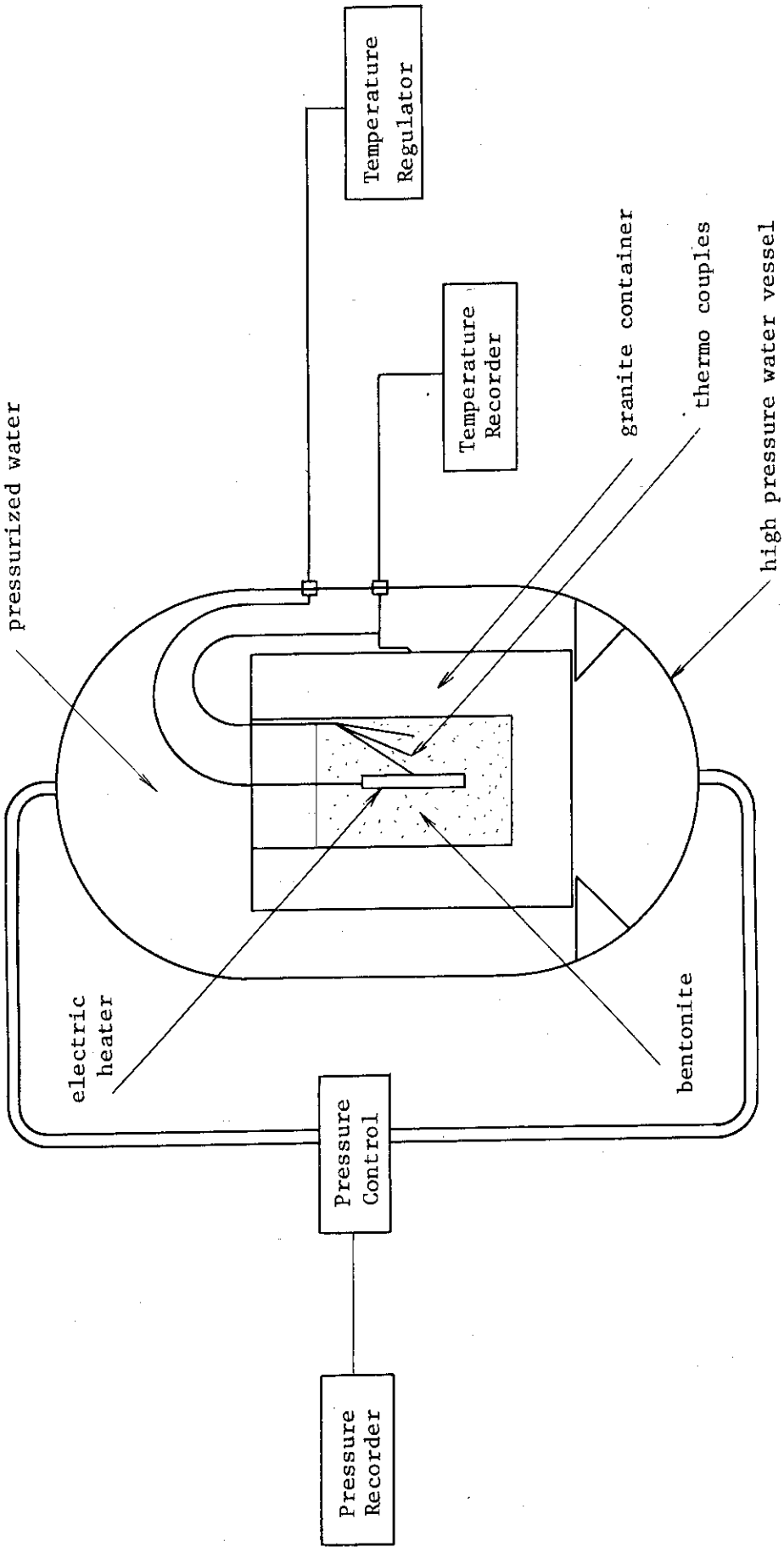

Fig. 1 Schematic diagram of system

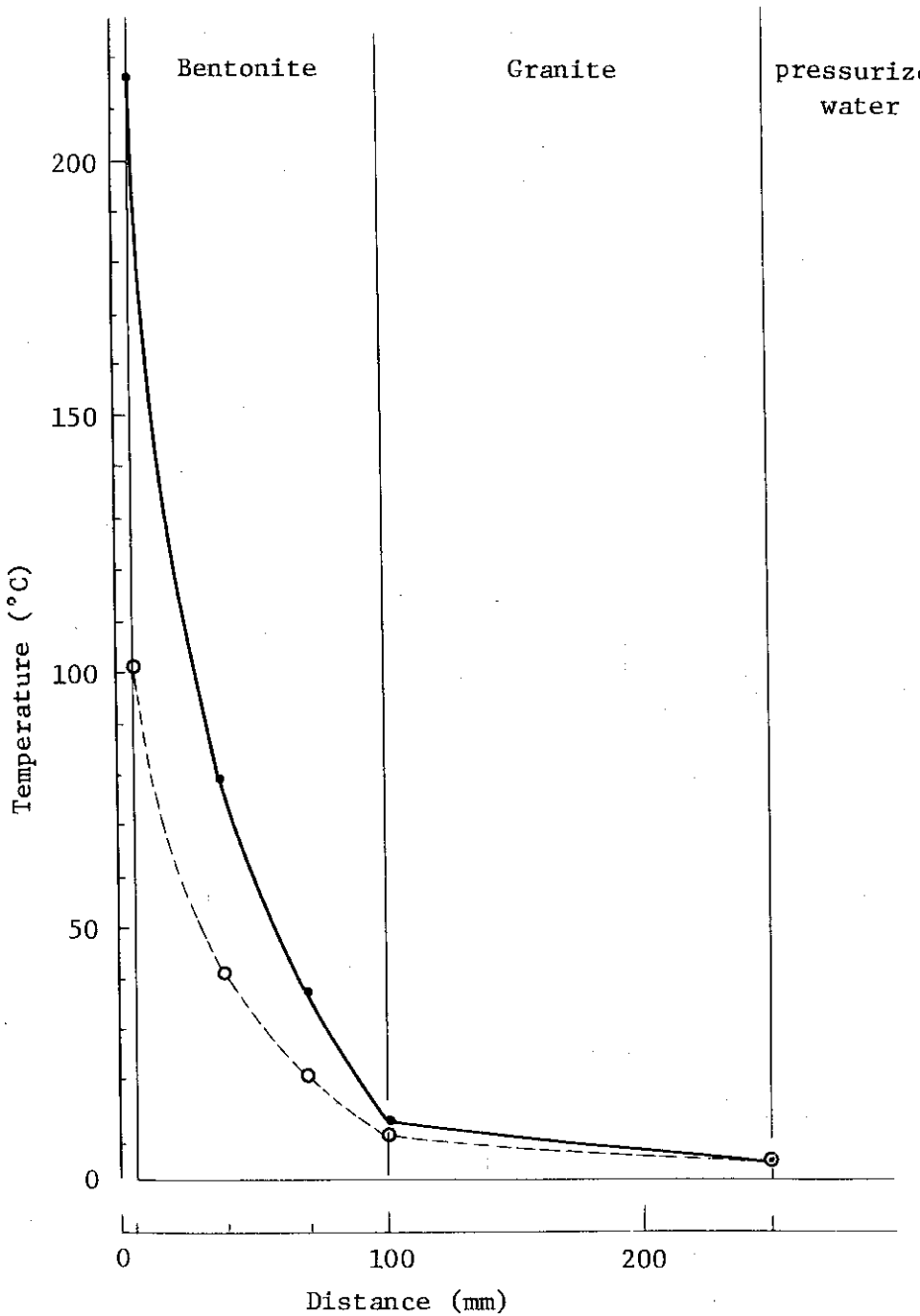

Fig. 2 Temperature Distribution at 50kg/cm^2

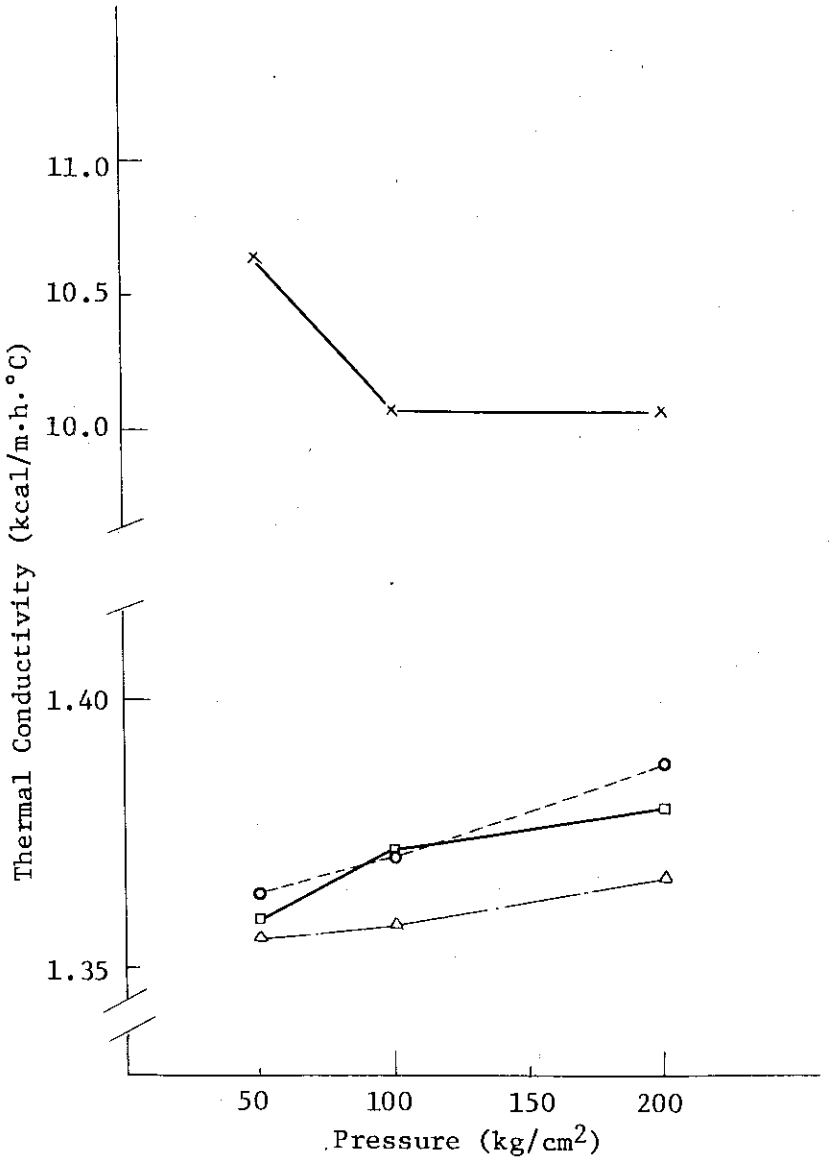

Fig. 3 Thermal Conductivity at 100°C Test

- r = 37 mm (in Bentonite)
- r = 69 mm (in Bentonite)
- r = 100mm (in Bentonite)
- r = 250mm (in Granite)

2.3.3 Diffusion of radionuclides into rocks

H. Nakamura and T. Yanagida

Migration of radionuclides in rock mass has been studied by many workers on determination of retardation factors for various rocks in laboratory and in-situ, permeability test of rock mass and developement of calculation codes. Their researches have been emphasized on models of retardation by ion exchange characteristics of rock.

We expect that the function of barrier of rock mass bases on the characteristics of rock as a water reserver for dilution and a reaction materials for mineralization of radionuclides. In order to define the place, where water is sunk and mineralized, diffusion test of typical radioisotopes contained in HLW into small blocks of granite was carried out, and red ink was permeated. Relation between porosity and distribution ratio was determined for various combination of rocks and radionuclides.

1. Diffusion test

Granite blocks of 5 mm thick, 10 mm width and 50 mm length were put on another to simulate a fracture. One end of the blocks were immersed in solutions of various nuclides, after distilled water was sorbed thoroughly into the blocks and polyethylene bottles were closed to prevent evaporation. The solutions were prepared by evapolation to dryness of acidic radioisotope solutions and dissolution with distilled water. After 11 days, the blocks were taken out from the bottle and broken to pieces of 10 mm X 10 mm X 5 mm. The radioactivities on both surfaces were measured by GM counter for ^{137}Cs and ^{90}Sr samples and proportional counter for ^{241}Am, ^{237}Np and ^{239}Pu.

The distribution of the activities are shown in Fig 1, where solid lines show the values for fissure surfaces and dotted ones for open surface. The acidities of the solutions were pH 5.5.

The activities of ^{137}Cs and ^{90}Sr decreased with distances from the bottom in exponentially as expected by diffusion mechanism, but ^{241}Am and ^{239}Pu were concentrated at the bottoms and ^{237}Np distributed all over the blocks.

This phenomena can be explained as follows. ^{241}Am and ^{239}Pu were liable to precipitate. The specific activity of ^{237}Np are low because of the long half life, 10^6 years. The concentration of the solution, 0.2 mg/ml, is too high for reaction capacity of rock.

Granite block sorbing the red ink showed that feldspar sorbs the ink homogeneously other than grain bounary.

2. Absorption of nuclides with various rocks

Japanese tipical rocks, granite, granodiorite, basalt, andesite and rhyolite were investigated on their absorability of radionuclides. Small samples 9.8 mm dia X 10 mm length were immersed in the solution of 0.7 ml containing radioisotopes by using a small polyethylene bottles. The blocks were sunk into water before the experiments. Porosities were measured by weight of sorbed water.

Distribution ratio (Kd) of radioactivities between the solutions and brocks were determined by using the activity concentration of the solutions before and after the absorption for 11 days as follows.

$$Kd = \frac{(C_0 - C_1)\frac{V}{M}}{C_1}$$

C_0 : initial concentration
C_1 : concentration after absorption
V : volume of solution
M : weight of rock

The results are shown in Fig. 2(b). The values of Kd was much smaller than the ones for powder of rocks. Only small part of brocks was used for absorption because of impermeability of crystalline grain of components of rocks.

Figure 2(a) shows the Kp, which is ratio between concentration in sorbed solution and free solution.

$$Kp = \frac{(C_0 - C_1)\frac{V}{Vp}}{C_1}$$

Vp : volume of water sorbed by rocks.

Kp is less dependent to sorts of rock than Kd, especially for ^{241}Am. This means that the porosity is an important factor for absorption of radionuclides by rocks. Our research will be emphasized on the grain boundary chemistry.

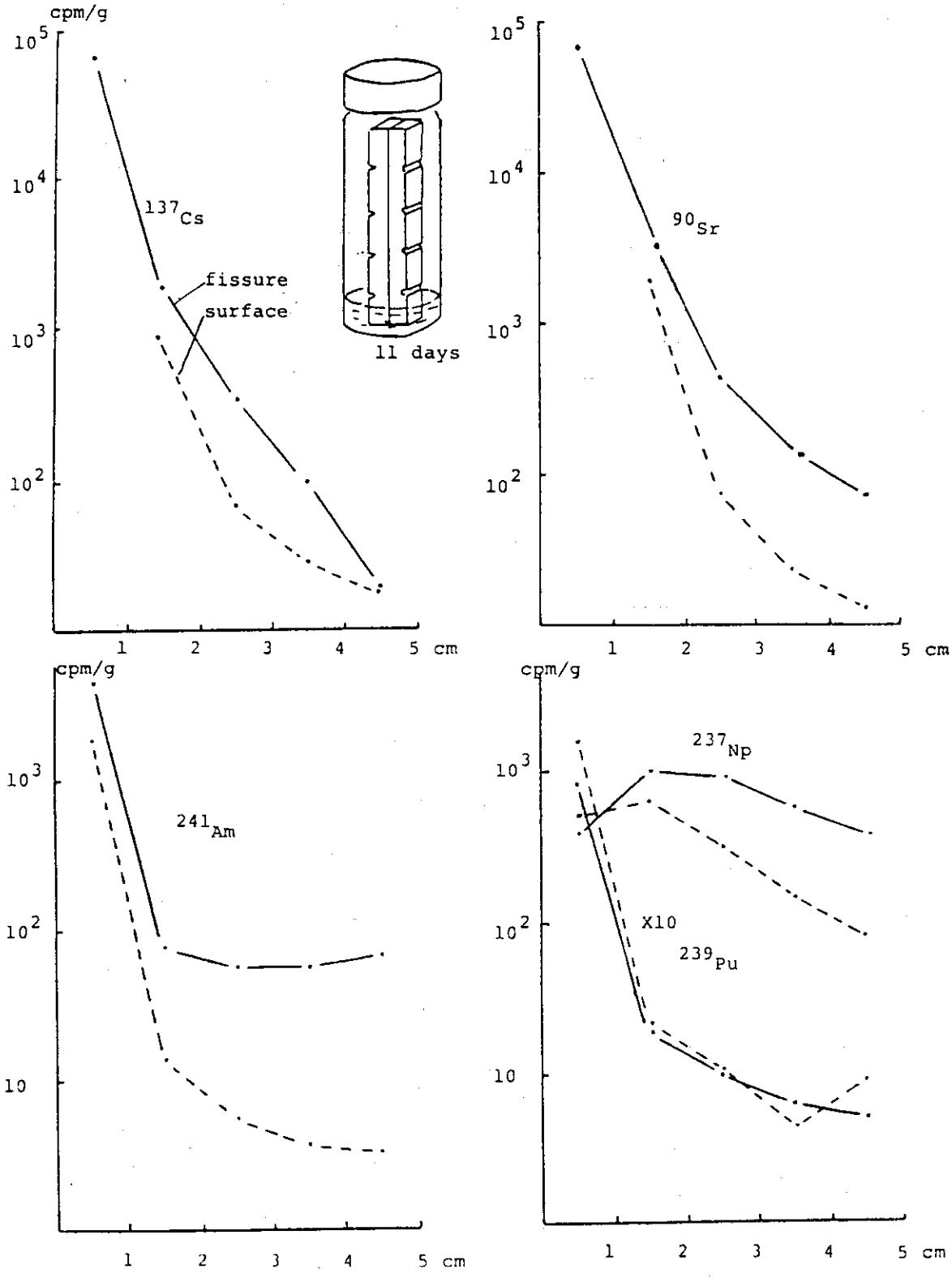

Fig. 1 Diffusion of nuclides to granite blocks

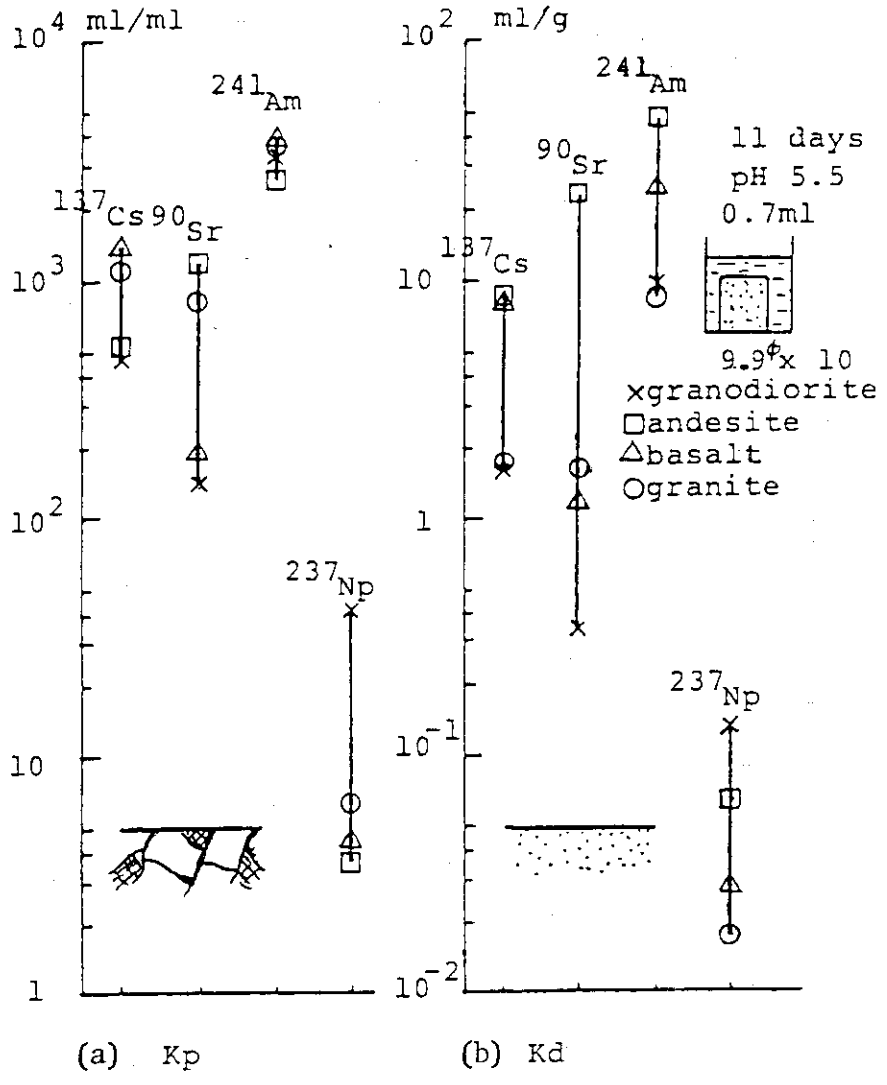

Fig. 2 Distribution ratio of various nuclides

2.3.4 Interaction of simulated high-level waste elements and rocks under hydrothermal conditions

M. Kumata

INTRODUCTION

The behavior of high-leval waste (HLW) elements has been investigated for the safety evaluation on a disposal option of solidified HLW in deep geological environments. The hydrothermal treatment of rock - simulated HLW glass - water system was used for understanding of physical and chemical change of rock, HLW glass and solution in the local geological environment of a waste repository, or near field, associated with the heat generation field of solidified HLW.

EXPERIMENTAL

The experimental details are described in earlier publication[1]. Briefly, the hydrothermal interaction was performed in batch method for closed system using deformable, inert, gold tube. The rocks, the simulated HLW glass and water used for this study were granite and basalt, a borosilicate glass containing 20 wt% simulated nonradioactive HLW and deionised water. Chemical compositions of solid materials used in this study were listed in Table 1. The samples were treated at the temperature of 100, 200, 300°C and at the pressure of 30MPa for 30 days.

RESULTS AND DISCUSSION

In the system, the behavior of the HLW elements in granite was similar to that in basalt. New crystalline phases including Cs were formed during hydrothermal treatment of both granite and simulated HLW glass, and basalt and simulated HLW glass. These phases varied in Cs concentration and were divided into two groups of element assemblage. One is consisted silicon, sodium, iron and cesium (see Fig.1). The other one consists of silicon, sodium, iron, aluminium and cesium with other rare earth elements.

Boron, an element forming glass network with silicon, almost completely dissolved in solution. Also, almost of molybdenum which was included in the simulated HLW glass as one of HLW elements was found in solution, but Sr was hardly detected in solution at all experiments.

From the above results, it is suggested that for the estimation of release amounts of HLW elements differences of igneous rock types play the role not so large. The rocks both granite and basalt played the role of catching the hazardous elements such as Cs and Sr released from HLW glass under these experimental conditions.

REFERENCE

1) Progress Report on Safety Research of High-Level Waste Management for the Period April, 1982 to March 1983, H. Nakamura and S. Tashiro (ed.), JAERI-M 83-076 (1983).

Table 1 Chemical compositions of solid materials

	granite	basalt	simulated HLW glass
SiO_2	73.19	49.77	51.19
TiO_2	0.15	1.74	
Al_2O_3	14.35	18.40	
Fe_2O_3	0.44	2.60	1.68
FeO	1.20	7.78	
MnO	0.26	0.18	0.27
CaO	1.79	8.11	
Na_2O	3.37	3.64	13.20
K_2O	4.58	1.13	0.01
P_2O_5	0.03	0.69	0.19
B_2O_3			21.31
Cr_2O_3			0.46
CoO			0.12
NiO			0.64
Rb_2O			0.13
SrO			0.34
Y_2O_3			0.39
ZrO_2			1.65
MoO_3			1.91
Ag_2O			0.02
CdO			0.02
Te_2O			0.16
Cs_2O			1.12
BaO			0.57
La_2O_3			0.40
CeO_2			1.39
Pr_6O_{11}			0.43
Nd_2O_3			0.90
Sm_2O_3			0.48
Gd_2O_3			0.40
Tb_2O_3			0.05
Dy_2O_3			0.22
Er_2O_3			0.03
H_2O^-	0.25	0.36	
H_2O^+	0.28	0.39	
Total	99.93	99.93	99.70

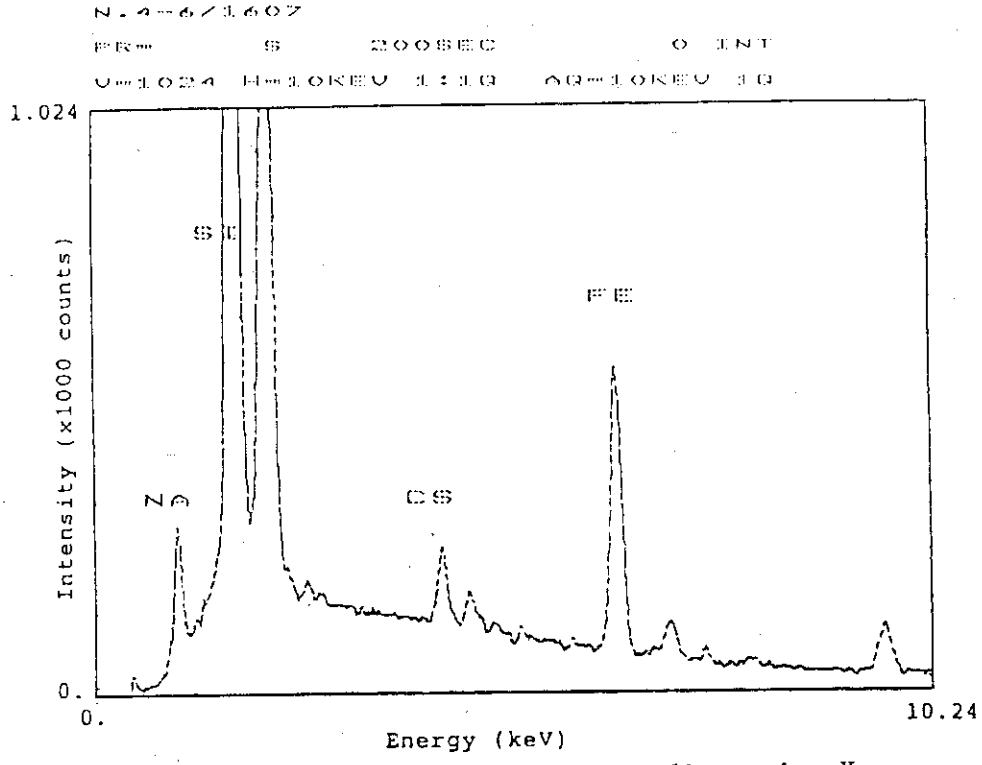

Fig. 1 Energy spectrum with energy dispersive X-ray analysis

2.4 Numerical model of flow and transport process in fractured-porous rock system

S. Muraoka

Introduction

Burial into deep and low permeable geological formations such as cristalline rocks is one of the solutions presently considered for the disposal of high level waste. Transport by moving groundwater is the most likely means of escape for released nuclide from the repository. For the assessment of the radionuclide transport, the modeling of water flow is critical importance in the geological disposal. The mathematical consideration of transient ground water in saturated-unsaturated porous media leads to the solution of initial boundary problem. We have developed numerical model by 3 dimensional finite element method.

Modeling

A general set of governing equations applicable to transport process in a fractured-porous medium can be derived from the basic consevation laws and Darcian flow concepts. As permeability at the fracture is given as a function of head pressure in our model, it becomes possible to treat the change of water flow due to elastic change of uncontinuous zone. Saturated-unsaturated seepage flow is described by the governing equations as follows:

$$-\nabla u + Q = C\frac{\partial h}{\partial t} \qquad \text{(continuous equation)} \qquad (1)$$

$$u = -[K_{ij}]\nabla h \qquad \text{(Darcy Law)} \qquad (2)$$

where

$u(r, t)$: Darcian velocity vector
$Q(r, t)$: source intensity
$C(r, h_p)$: specific moisture capacity
$K_{ij}(r, \theta)$: permeability tensor
$h(r, t)$: total head
r : position vector
t : time

Permeability tensor K_{ij} is given by equation (3)

$$K_{ij} = \mathring{K}_{ij} \cdot k\ (h_p, \theta) \tag{3}$$

where

$\mathring{K}_{ij}$: saturated permeability tensor

$k\ (h_p, \theta)$: unsaturated permeability coefficient

As a model expressing the permeability in the discontinuous media, double porosity model was developed by J.E. Wareen et al.. It is difficult to use the double porosity model directly in our model because of 3 dimensional steady state analysis. In order to simplify the calculation it was introdued the searing model. In this model fractures are not fixed at the specific site in the element but dispersed in the element. Flow velosity in the element is given as follows

$$u = -K_s\, vh \qquad \text{(in solid)} \tag{4}$$

$$u = K_f\, vh \qquad \text{(in fracture)} \tag{5}$$

where

K_s : permeability tensor in solid

K_f : permeability tensor in fracture

K_f is assumed to be homogeneous in the fractured area.

$$\alpha \int v\bar{u}_s \cdot dxdydz + \int v u_f W dxdy = \int v(d\bar{u}_s + u_f \cdot p) \cdot dV \tag{6}$$

where

p : scaler $Wdx \cdot dy/dxdydz$ = volume ratio

α : constant

From this treatment, fractures were modeled by the volume ratio in each element.

The general solutions of the governing equations were obtained using numerical models. Numerical models were base on a Galerkin finite element technique of weighted residuals.

Numerical result

Calculated result with input data is shown in Fig. 1.

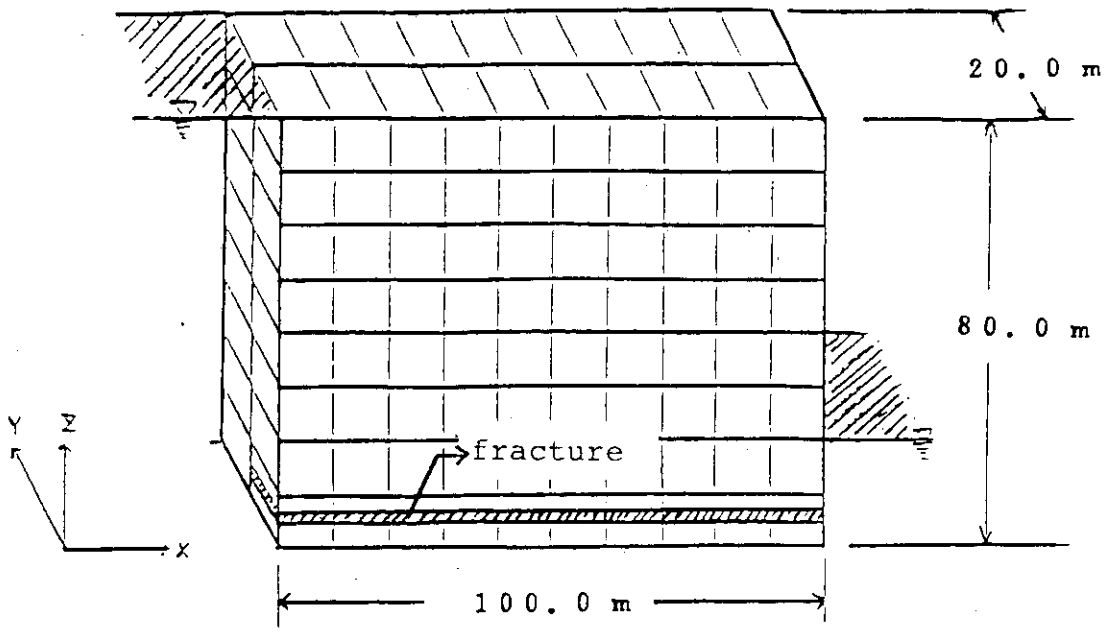

permeability in solid	0.00085 m/day
permeability in fracture	0.85 m/day
volume ratio of fracture to solid	0.1 %

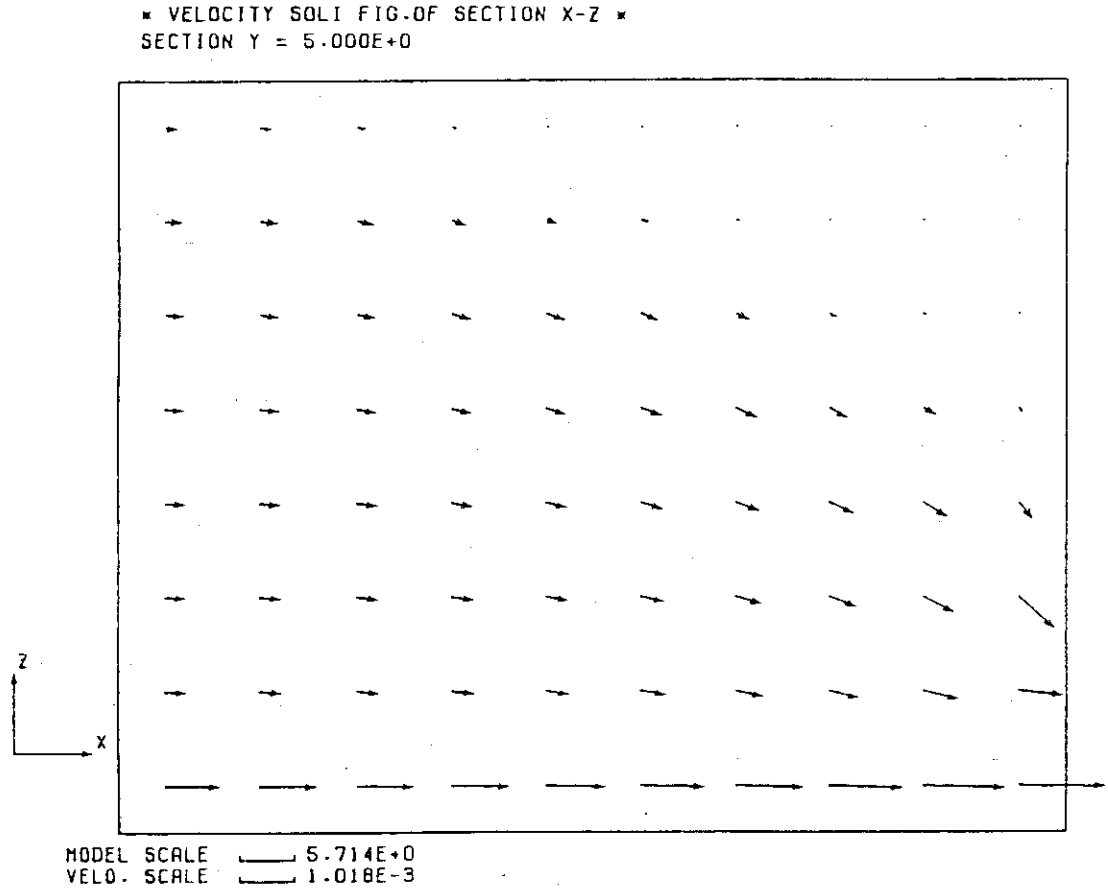

Fig.1 Example of water flow

3. Safety Examination of Vitrified Forms in the Hot Cells of WASTEF

S.Tashiro

The Waste Safety Testing Facility (WASTEF)* has five concrete shielded hot cells to examine the safety performance of high-level waste management technologies using radioactivity of similar concentration to real wastes.

In this fiscal year, eleven radioactive vitrified products have been prepared for the use of safety examination in the hot cells. Main items of the examination performed in the year are given as follows:

(1) Compatibility test of near field materials under gamma-ray irradiation

The details should be refered to in the section 2.3.1.

(2) Dispersion test of powdered vitrified forms

The details should be refered to in the section 3.2.

(3) Volatilization test

For the safety assessment under unusual storage conditions,

---

* The design and specification would be refered to in the report of S.Tashiro et al : JAERI-M 83-175 (Oct. 1983) (in Japanese).

volatilization behaviour of vitrified high-level wastes has been examined using Cs-134, Cs-137 and Sr-90 in No.1 Cell. In the year, concentration of volatiled radioactivity in a closed atmosphere contact with the vitrified form surface has been measured at various temperatures upto 1,000 C.
Radioactivity defused out from crucibles containing vitrified HLW has been also measured at various temperatures upto 1,000 C.

(4) Leaching test

Leachability of Pu-238, Sr-90 and Cs-137 has been measured for a vitrified form with Soxhlet method apparatus installed in the No. 4 Cell .

(5) Alpha radiation stability test

Alpha radiation stability test was started July 1984 using Cm-244 of 80 Ci and Pu-238 of 9 Ci in No.5 Cell. It will continue till July, 1985 when the density of alpha disintegrations in the vitrified form is equivalent to the real waste form aged 10,000 years.
Above items of (3),(4) and (5) have been performed for the characterization of high-level waste forms to be returned from the oversea-reprocessing. The related items should be refered to on the whole in the section 3.3.

(6) Development of gamma-scanning system for homogeneity examination of vitrified forms

The details should be refered to in the page section 3.4.

3.1 Production of radioactive vitrified test samples

J.Morita

Eleven radioactive vitrified products have been prepared for safty tests in this current year including four ones made with vitrification apparatus. Table 1 gives an outline of these runs with the apparatus.

Each sample was made from synthetic wastes(simulated wastes partially replaced with radioisotopes), which were feeded directly into melter and treated by the processes of calcination, melting, conditioning and off-gas treatment.

The operating condition of calcination and melting has been modified by increment of the heating capacity of freeze valve zone so that glass was molten and discharged to a receiver in seven hours after start up of heating.

A temperature obtained by the new heater is 1160 °C in maximum and it took 2 hours and 40 minutes to the maximum temperature.

Surface contamination in the cell after each run was measured by smear method. As a result of the measurement, feature of shutter which is placed between melter and receiver, was improved after the run of H83005 for the purpose of preventing that vapor of molten glass had been escaping from the housing (Fig. 1).

Radioactivity of meterial catched in off-gas line, was

measured to confirm the performance for off-gas treatment (Fig. 2).

Fig. 2 shows that the amount of radioactivity removed at scrubber was increased largely after the run of H83005 and the improvement would be effective.

Table 1 Specification of vitrification

Run No.	Composition of product			Weight of product (g)	Purpose of production
	Matrix	Waste (Content,wt%)	RI (Activity,mCi)		
H83001	COGEMA	JW-C (17.5)	Mo-99 (839)	1331.0	Powderization behavior test
H83005	COGEMA	JW-A (17.5)	Cs-134 (511)	1171.0	Volatilization behavior test
H83006	COGEMA	JW-C (17.5)	Mo-99 (1700)	1209.0	Powderization behavior test
H83009	COGEMA	JW-C (17.5)	Cs-137 (400)	2079.0	Reference sample

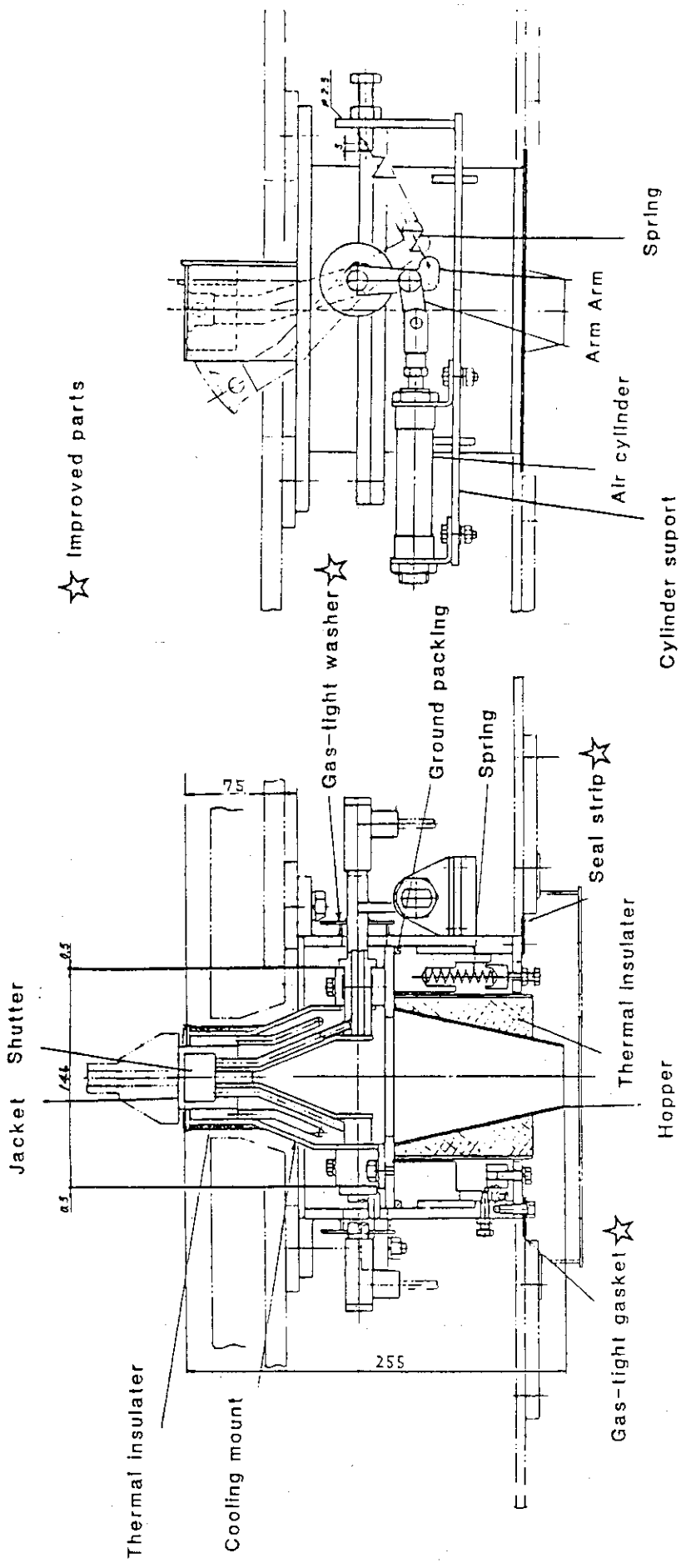

Fig. 1 Improved feature of shutter

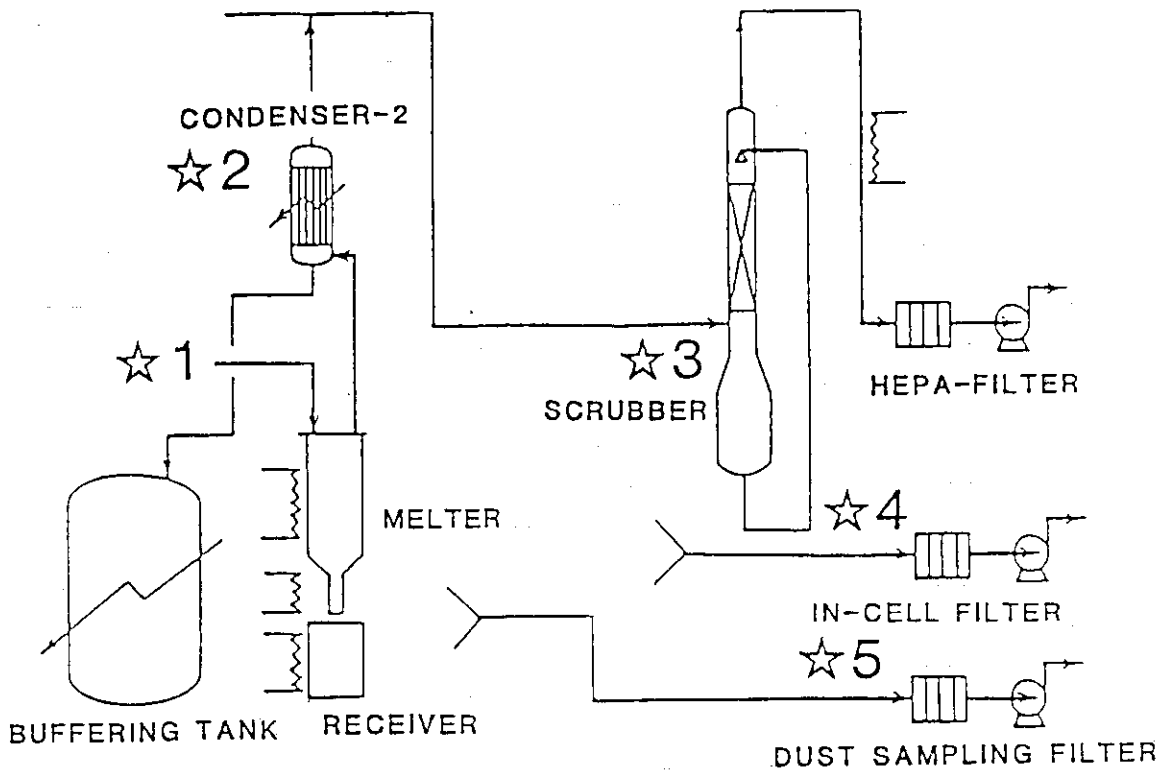

Run No.	Feed ☆1 (mCi)	Cond. ☆2 (μCi)	Scrub. ☆3 (μCi)	Cell ☆4 (x 10^{-11}Ci)	Melter ☆5 (x 10^{-9}Ci)
H83001	830	4.5	41.0	96	110
H83005	511	13.0	12.9	—	—
H83006	1700	160	5000	—	—
H83009	400	9.7	2600	—	—

Fig. 2 Activity distribution in down stream

3.2 Study of HLW glass powderization behavior

T. Takeda

To solve difficulties in estimations of ambient contamination levels inside the storage facilities under normal and accident conditions, as fundamental information to accept returned-vitrified HLW from oversea reprocessing of spent fuels, two researches have been set up. These are (1) glass fracturing behavior and (2) glass particle behavior after and during powderization. The first has been developed on the item of "Glass crushing behavior evaluation code : ADEKAT-G". Another has been studied by a experimental procedure described in this section. Major object of this work is to clarify experimentally the ambient contamination limits for actual glass waste.

Two powderization experiments have been done using Mo-99 of 7 Ci and Cell #3 in WASTEF. The glass (0.5 l) was crushed in the Cell #3 and powderized glass particles were sampled from a sampling head. The particles were collected on the each plate of a cascade impactor and the particle size distributions and the radioactivities were measured by the impactor and by a multichannel pluse height analyzer respectively. Outline of experimental system and obtained data are shown in Figs. 1, 2 and 3. Maximum value of particle density suspended in ambient is lower than 3 mg/m^3 and peak in size distributions is 1.5 - 0.4 μm approximately.

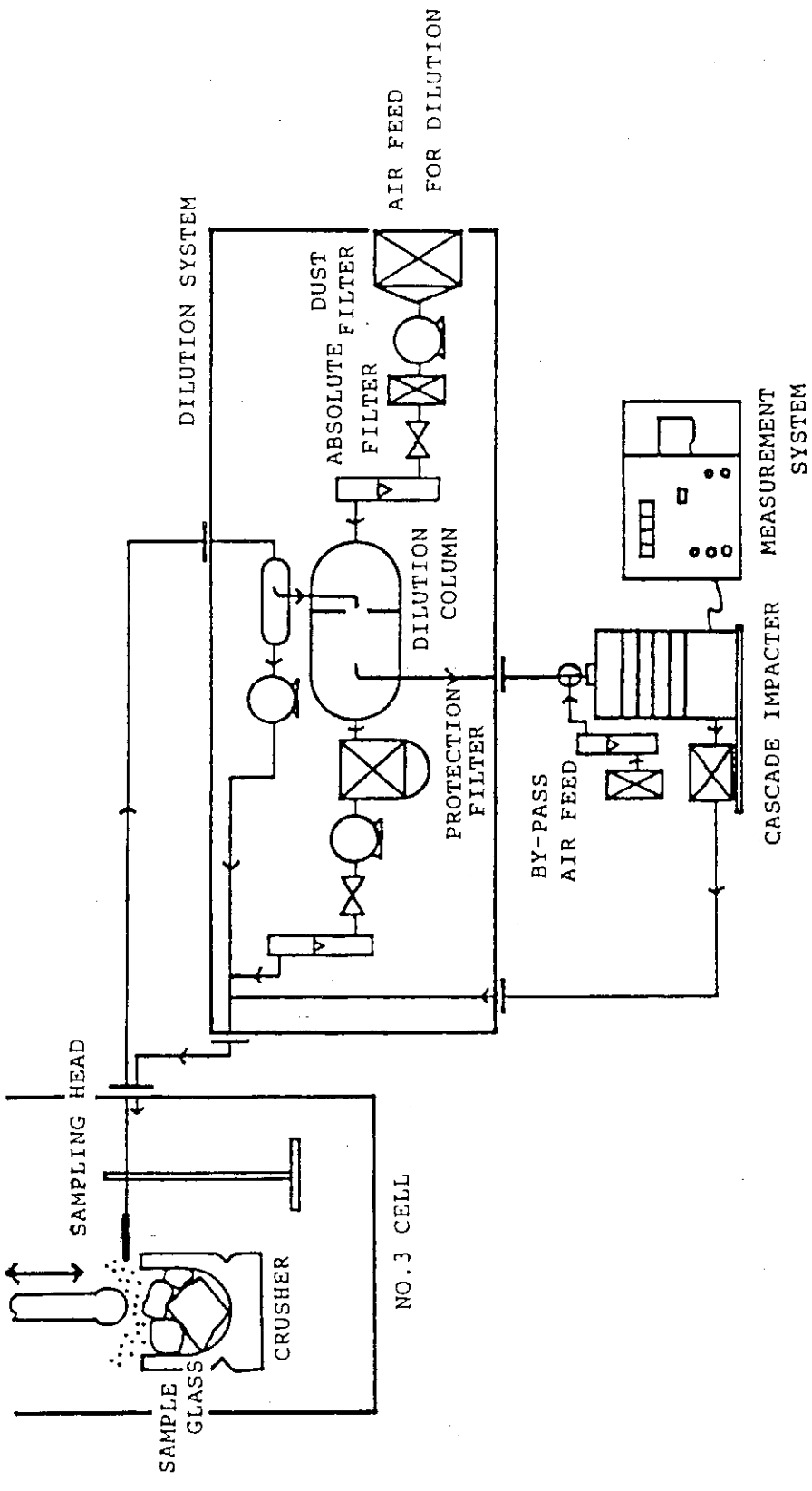

Fig. 1 Flow diagram of glass dispersion behavior test apparatus

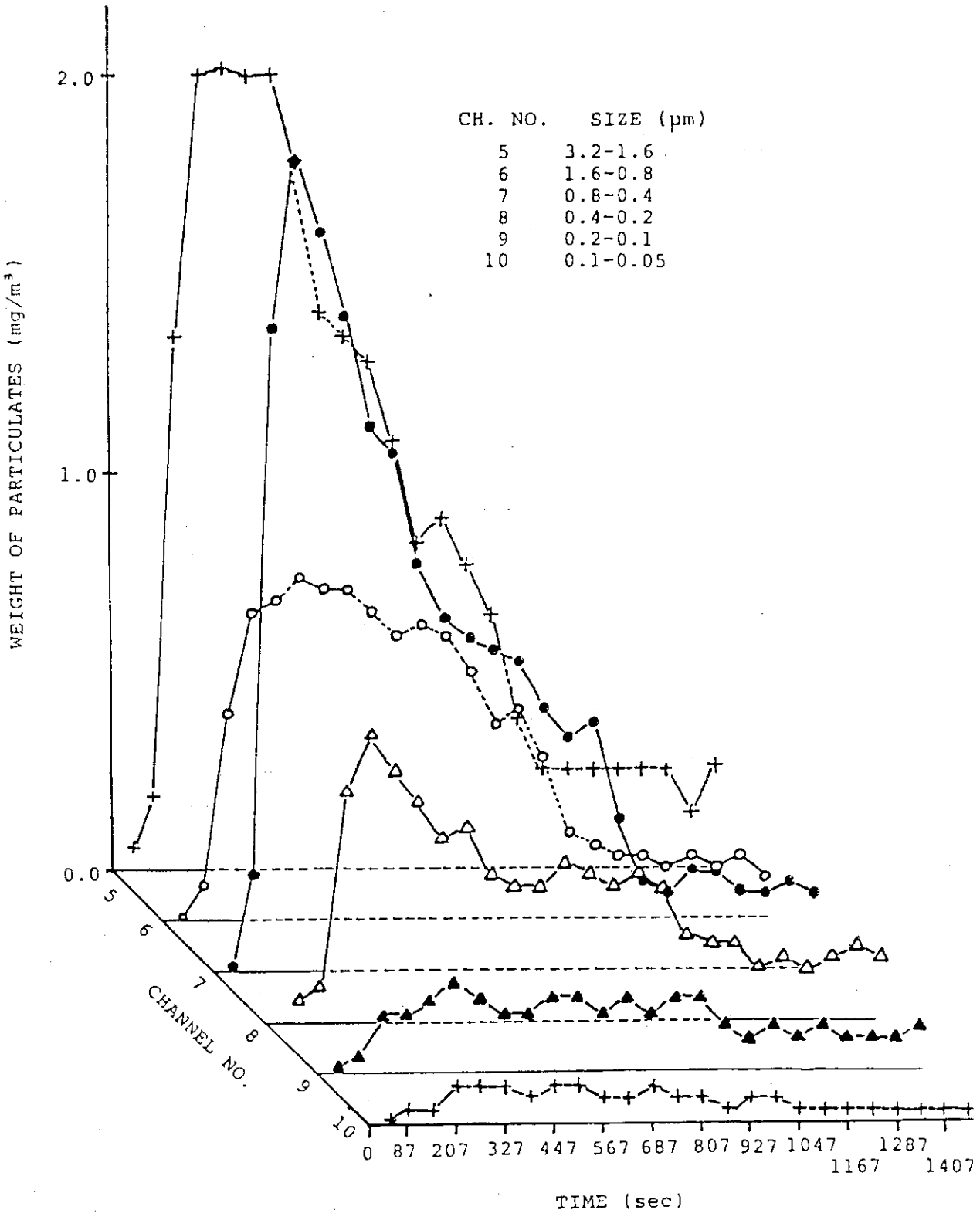

Fig. 2 Size distribution of crushed glass

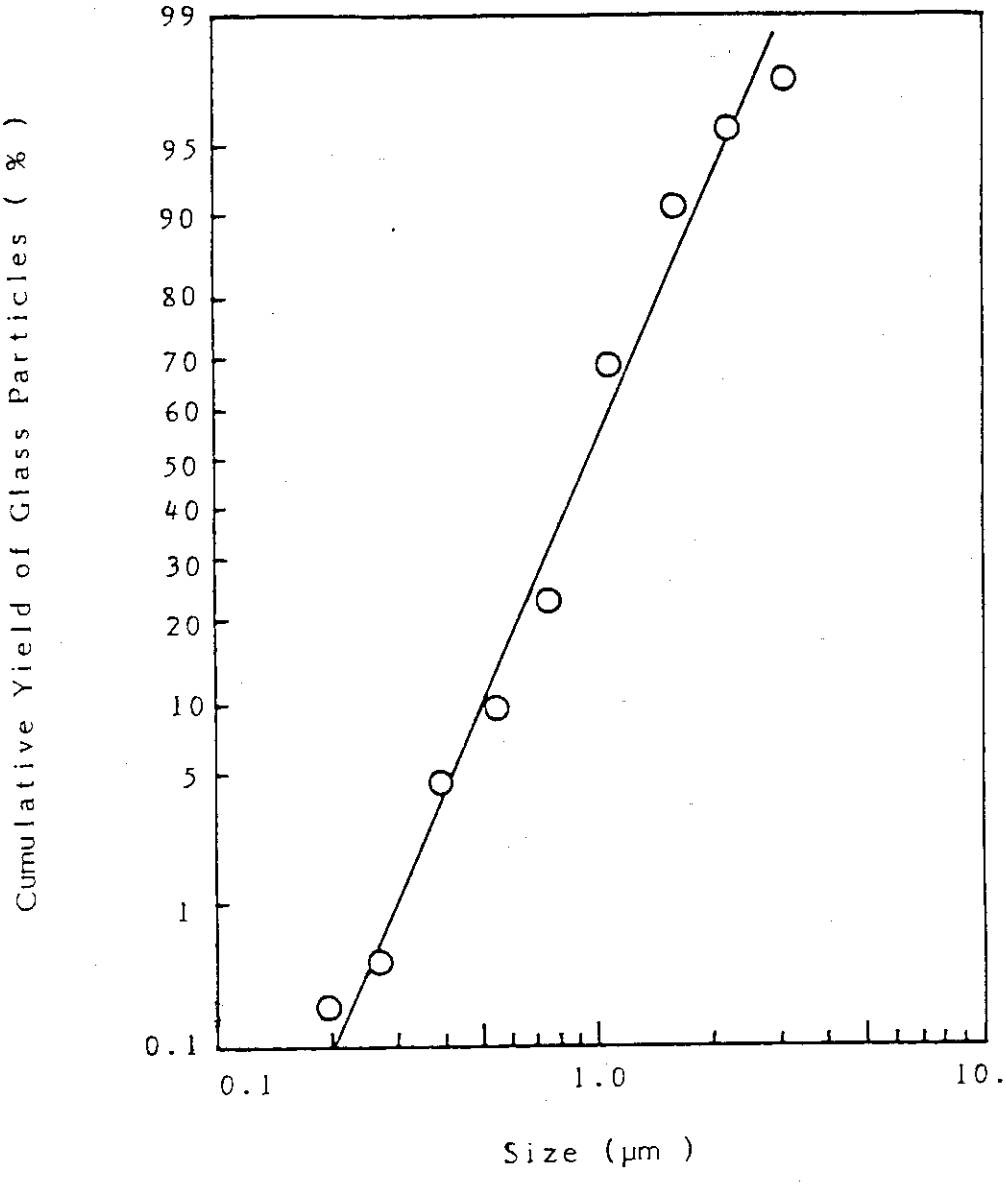

Fig. 3 Size distribution of glass particles suspended in ambient atmosphere (Log-normal distribution scale)

3.3 Characterization of waste form to be returned from over-sea reprocessing

Y. Kiriyama

Characterization tests of the HLM vitrified form to be returned have been continued.

In this fiscal year, the following items have been investigated.

1) The compositions of the test samples were determined with the experience of the cold examination using simulated fission products and actinide elements and the convenience to use radio nuclides.

After the preparation of test samples, the analysis of composition were carried out by X-ray fluorescence analysis instruments.

2) The preparation of test samples were performed for the α radiation stability test using short-lived α emitters (Cm-244 and Pu-238). The doped amounts of α emitters was calculated due to TRU concentration in the real waste form.

First of all, the preliminary characterization test of the samples was carried out and the rest of samples has been stored in the capsules filling up with Ne gas.

3) In order to know preliminary informations about the damage of vitrified form by α radiation, changes of the vitrified form in the following items was measured before and after neutron irradiation

- o dimension
- o density
- o leachability

The irradiation was carried out in the Japan Materials Testing Reactor, Oharai Establishment, JAERI, and expected to emit α radiation by (n,α) reaction in the forms.

4) The volatility tests of the forms using Sr-90, Cs-137 were performed.

5) The leachability tests of the forms using Sr-90, Cs-137 and Pu-238 were performed in the Soxhlet type devices.

3.4 Development of Gamma-scanning System for Homogeneity Examination of Vitrified Forms

M. Nomura

1. Introduction

A gamma-scanning system has been developed to estimate the radioactive homogeneity of vitrified forms prior to tests on the safety properties such as leachability, volatility etc., which are influenced by the homogeneity. The system is characterized by automatic mode for operation and homogeneity estimation obtained nondestructively by a computed tomography technique.

2. System Discription

The system consists of gamma-scanning hardware and software for the system control and the data processing. The block diagram of the system is shown in Fig. 1.

The components of gamma-scanning hardware are:

(a) an in-cell sample positioning apparatus

(b) a collimator plugged in the concrete shielding wall

(c) an intrinsic germanium detector

(d) a system computer.

The system is operated in automatic mode by the computer after a set of parameters for scanning intervals and radiation measuring time has been fixed. The scanning intervals for each measurement are 1 mm for translation and 1 degree for rotation movement at minimum.

Three sizes of aperture are available to collimate gamma-rays and one of them is selected owing to the radioactive concentration of the form.

The intensity of gamma-rays through a collimator is measured by the intrinsic germanium detector which has almost equivalent characteristics to the lithium drifted germanium detector without the need for constant cryogenic cooling.

The system computer is used to control the in-cell sample positioning apparatus, to collect data of radiation measurement, to calculate the integral peak activities of selected nuclides from the data and to store the activities on magnetic tapes. The jobs are performed sequentially at each scanning position interval.

The specifications of components are listed in Table 1.

In order to estimate radioactivity concentration of each nuclide in the form, the data on magnetic tape are reconstructed rapidly by the host computer installed at the computing center in the Tokai Research Establishment, JAERI, using a data processing code which can correct the material absorption effect of gamma-rays and reconstruct the corrected results by a convolution method.

3. Function Tests

After confirming the performance of the gamma-scanning hardware, function tests for data processing has been carried out

in the following two steps; (1) simulation test, (2) demonstration test using a vitrified form with Cs-134.

A set of simulated data calculated under a condition of assumed radioactivity distribution in the form (Fig. 2) was used for the simulation test. Because a gamma intensity attenuates by passing through the vitrified form and canister, it is necessary to correct this material absorption effect prior to the reconstruction. The effect was corrected by using equations proposed by Sorenson and Keyes respectively. The corrected data were reconstructed by a convolution method using Ramachandran's, Shepp & Logan's and Chesler's filter function respectively. It has been found that the combination of Sorenson's equation and Shepp & Logan's filter function has been applicable to our calculation after the investigation of 6 reconstructed results from combinations of the equation and the filter function. The reconstructed results are shown in three dimensional display in Fig. 3. It becomes clear from the figure that a 2 mm diameter radiation source can be detectable and the figure becomes to have rather rounded shoulders on the boundary where the steep changes of radioactivity concentration occur in a very narrow region.

A vitrified form with Cs-134 was used for the second step test. This sample was prepared by inserting the Cs-134 source into three holes of a cold vitrified form which was core-drilled in three positions. The cross sectional view of the sample is shown in Fig. 4. Gamma-ray intensity was measured by the scanning

interval of 2 mm translation and 6 degree rotation movements. The reconstructed figure is shown in Fig. 5 which was obtained by the same analysis to the simulation test. The position of Cs-134 sources are exactly distinguished in the figure. However, the figure shows rounded shoulders as well as in the reconstructed results of the simulation test on the boundary where steep changes of radioactivity concentration occur.

In conclusion, it has been found that the system developed is applicable for the estimation of radioactive homogeneity by using a computed tomography technique.

Future work will be concentrated on improving the system to have more sharp reconstructed figure and reducing time for gamma-scanning measurement.

Reference:

1) H. Otsuka, Y. Tamura, M. Nomura, S. Tashiro, "Development of Gamma-scanning System for Homogeneity Examination of Vitrified Forms", JAERI-M84-067 (1984)

Table 1 Specifications of components

Components	Specifications
Positioning apparatus	Scanning range : X = 0∿85 mm Y = 0∿45 mm Z = 0∿300 mm θ = 0∿360° Scanning interval: translation min.1mm rotation min.1°
Collimator	Material : Antimonial lead Dimension : 100mmϕ × 250mmℓ Aperture : 0.3, 0.5, 1.0
Germanium detector	Energy Resolution : 1.73 keV at 1.33 MeV Efficiency : 0.18 compared to 3"×3" NaI at 1.33 MeV
Computer	PDP11/03 (64 kbyte memory) with cartridge disk, floppy disk, magnetic tape and printer

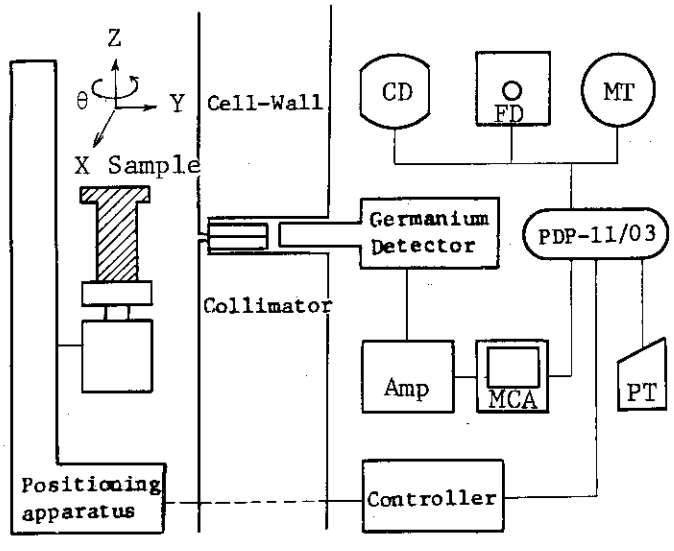

data acquisition & system control

MCA: Multi-channel analyzer
CD: Cartridge disk
FD: Floppy disk
MT: Magnetic tape
PT: Printer

Fig. 1 Block diagram of the system

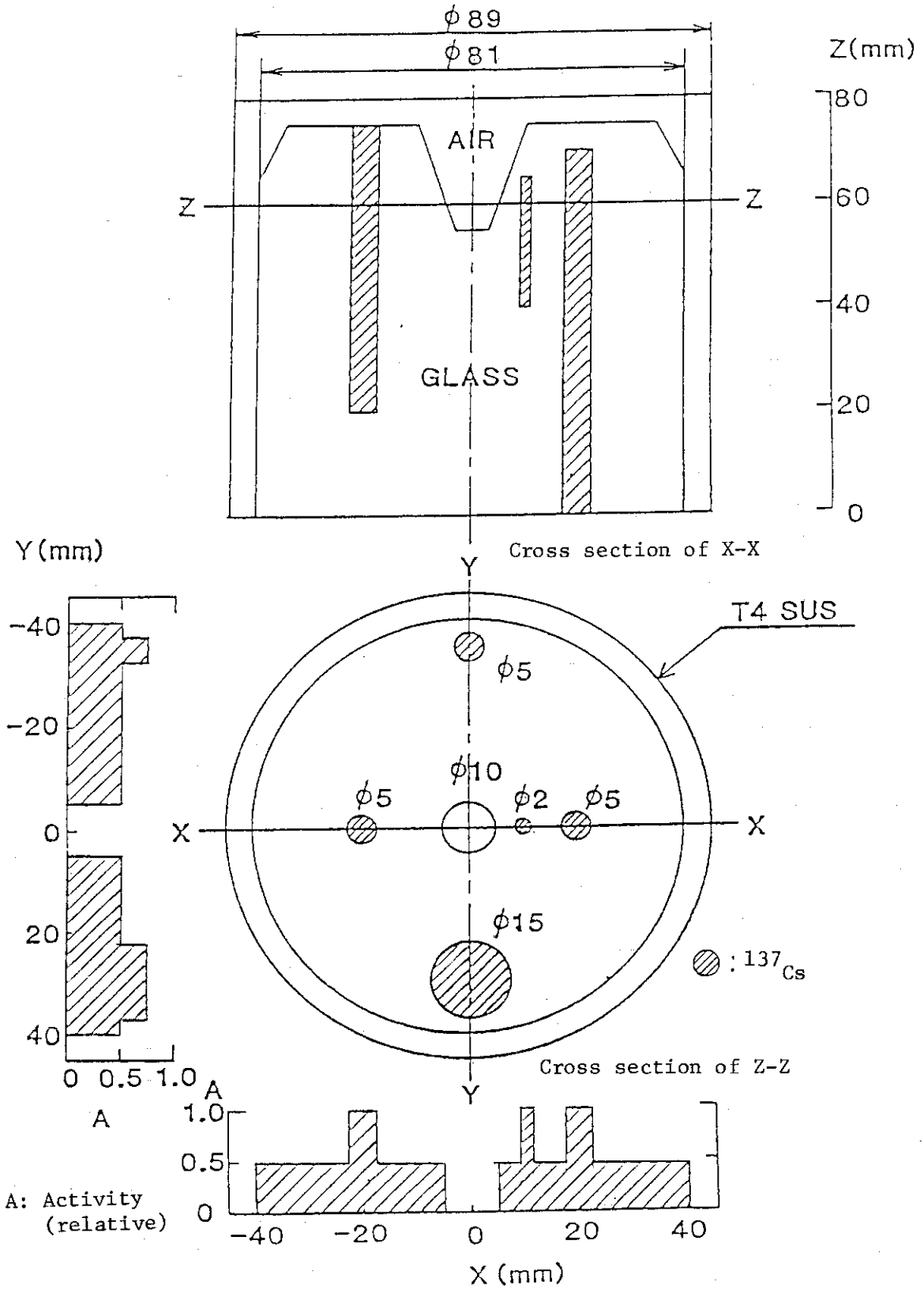

Fig. 2 Radioactivity distribution in the form for simulation test

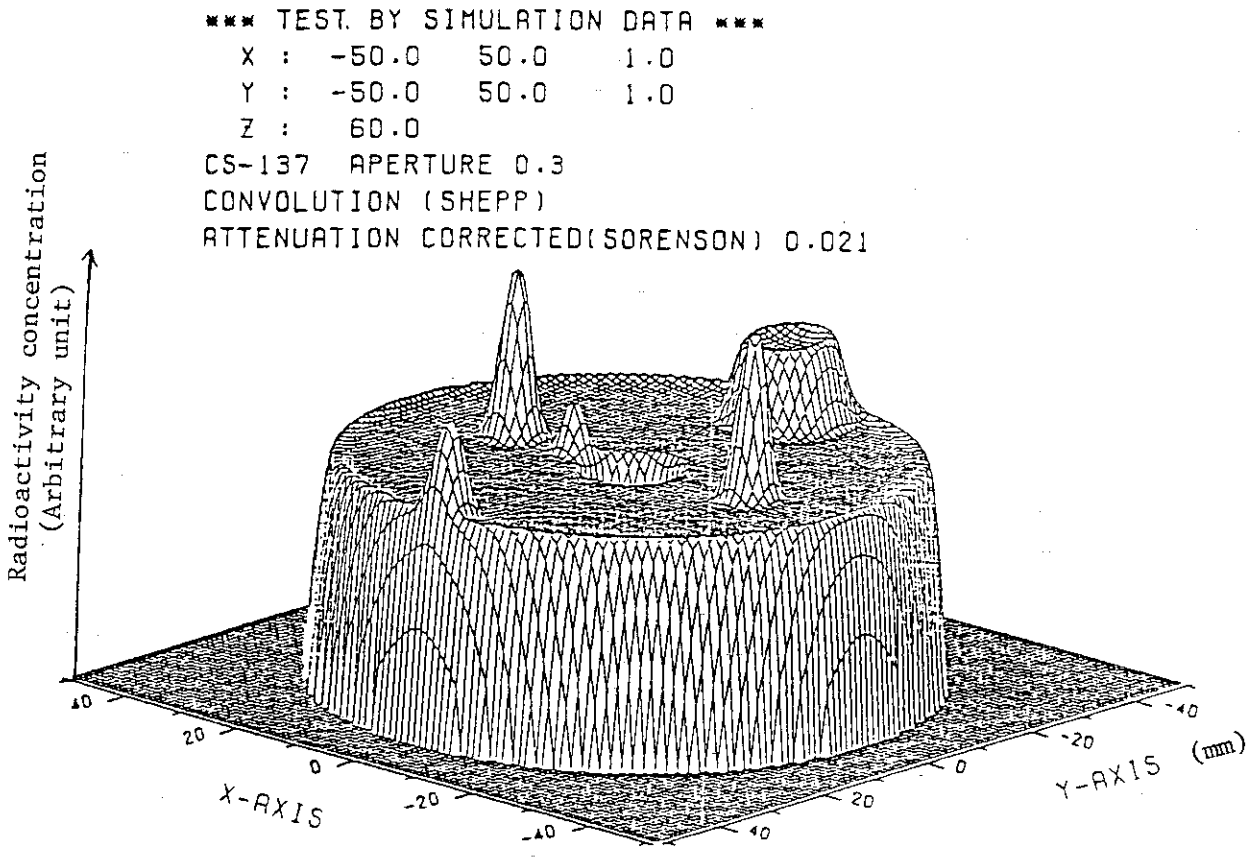

Fig. 3 Reconstructed figure of the simulation test

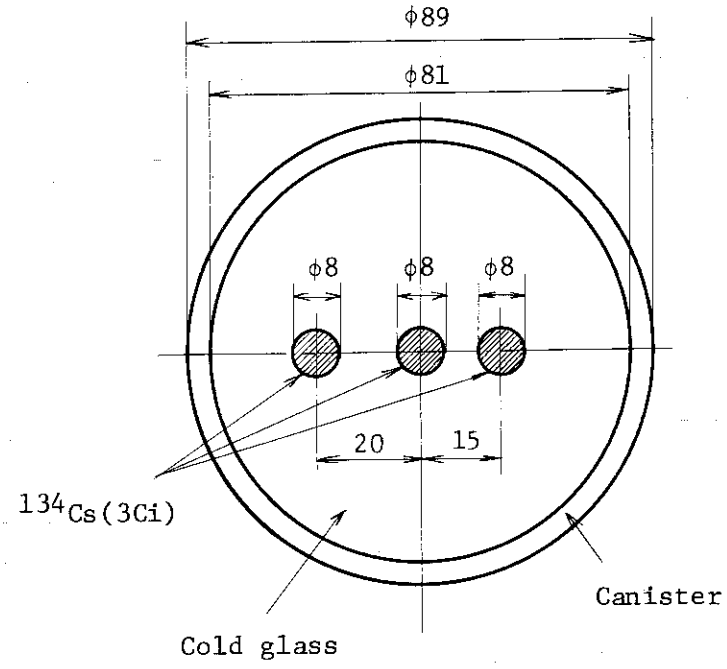

Fig. 4 Cross sectional view of ^{134}Cs contained vitrified form for the demonstration test

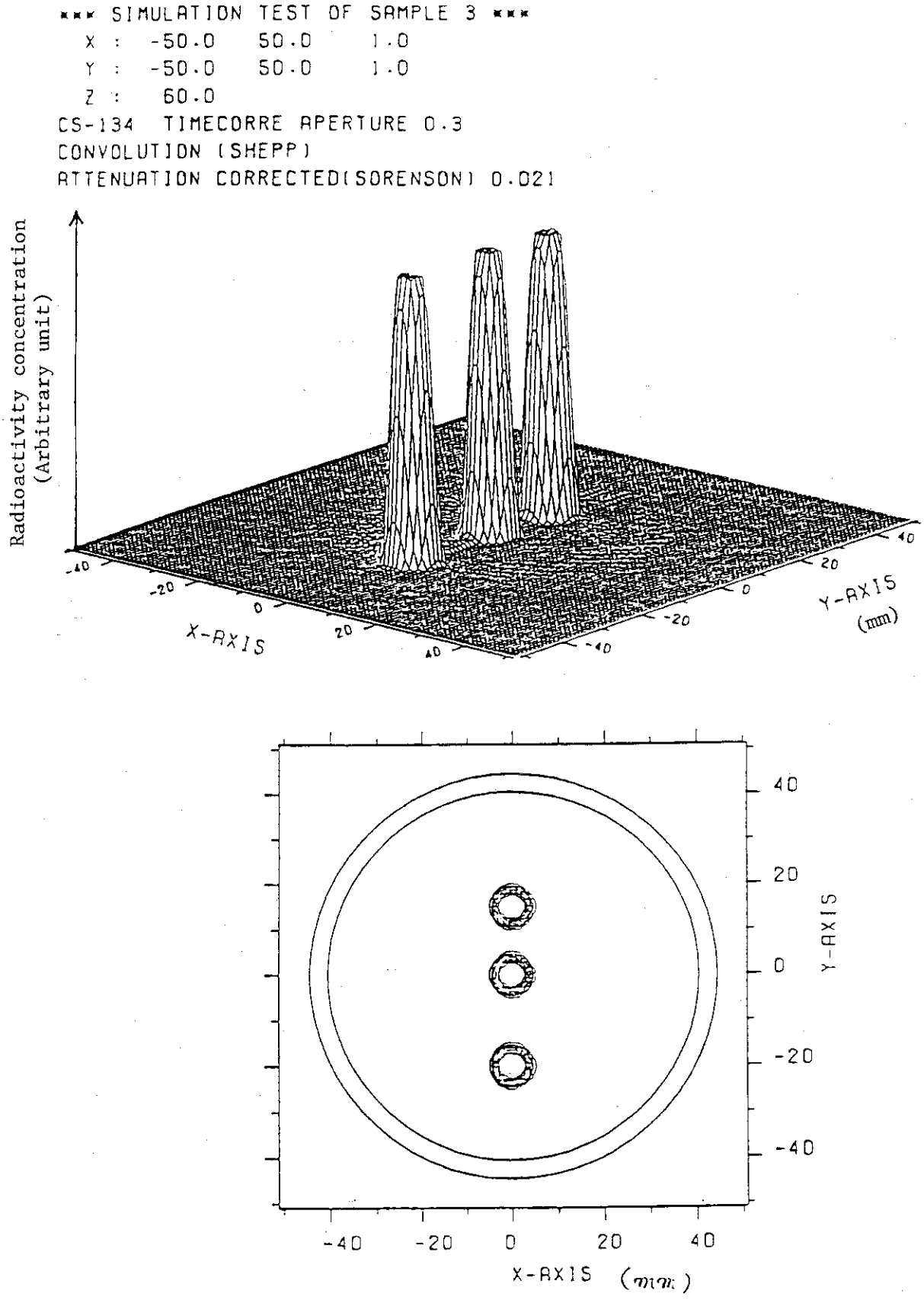

Fig. 5 Reconstructed figure of the demonstration test

4. Safety study of nuclear facilities of vitrified HLW's stream

T. Takeda

One of the problems to be solved urgently is to establish safe storage and transportation of returned-vitrified HLWs. The Japanese power companies and their organized committee is conceptually designing the waste storage facilities and shipping packages. The regulatory bodies will have to study the safety of the facilities. In order to support the regulatory bodies, safety evaluation methods have been studied and a committee was held to discuss the program and results of research items. The committee consists of specialists of our institute, nuclear industries and universities. In this year, (1) a document set supporting the actual waste storage facilities in the future has been tentatively prepared in JAERI, and (2) research items have been picked up and discussed based on the former document set in the committee.

As for the first, the tentatively-referential document set has been compiled using present regulation application forms and using present safety examination requirements. Therefore, the set consist of two parts: (1) main text of safety analysis report, and (2) technical backup materials, supporting to the former part. Assumption of the storage facilities used are (1) dry storage, (2) air-cooling and (3) under normal and accident conditions. And the set covers on field of (1) structural, (2) thermal, (3) containment, (4) radiation shielding and (5) critical safety analysis and assessment. In addition, the results of applicabilities studies of existing computer codes obtained last year are added to the later part as numerical basis for the assessment.

As for the second, the committee has picked up and discussed on weighing of research items. Many critical points on safety research of HLWs storage facilities are picked up based on the tentatively-referential document set. One of typical problems is to solve containment safety evaluation and to collect its technical data, especially glass powderization behavior. The results of glass powderization experiments are descrived in other pages. And glass cracking analysis is also one of typical problems. Deformation analysis code "ADEKAT-G" developed in last year has been versioned up in this year, especially in order to solve contact problem. Another points is to solve the air contamination coming from the contaminated surface of the canister. The most probable contamination will be induced by the sublimation of Cs radionuclide. Study on the characteristics of sublimated Cs is also important items and is started in No. 1 Cell of WASTEF.